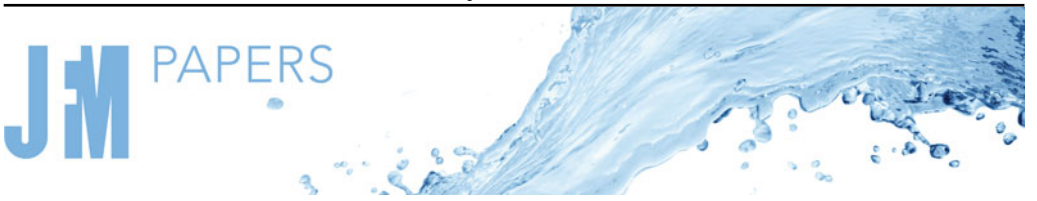
J. Fluid Mech. (2026), *vol.* 1028, A34, doi:10.1017/jfm.2026.11135



High-order strongly nonlinear long wave approximation for variable bottom

Wooyoung Choi[1] **and Sunao Murashige**[2]

[1]Department of Mathematical Sciences, New Jersey Institute of Technology, Newark, NJ 07102-1982, USA

[2]Department of Mathematics and Informatics, Ibaraki University, Mito, Ibaraki 310-8512, Japan

Corresponding author: Sunao Murashige, sunao.murashige.sci@vc.ibaraki.ac.jp

(Received 17 July 2025; revised 24 November 2025; accepted 1 January 2026)

This paper describes a high-order strongly nonlinear (SNL) model for long waves in the presence of a variable bottom, which is a generalisation of the model for a flat bottom (Choi 2022*a*, *J. Fluid Mech.* vol. 945, A15). This asymptotic model written in terms of the bottom velocity is obtained using systematic expansion with a single small parameter measuring the ratio of the water depth to the characteristic wavelength and is found linearly stable at any order of approximation. To test the high-order SNL model with a variable bottom, we solve numerically the first- and second-order models using a pseudo-spectral method to study the deformation or generation of long waves over a variable bottom. Specifically, we consider two examples: (i) the propagation of cnoidal waves over a fixed bottom topography, and (ii) the forced generation of solitary waves by a submerged topography moving steadily with a transcritical speed. The computed results are then compared with the fully nonlinear computation using a boundary integral method as well as the numerical solutions of the weakly nonlinear long wave model. It is found that the second-order SNL model for the bottom velocity is suitable for stable numerical computations and produces accurate solutions even for a relatively large-amplitude initial wave or submerged topography.

Key words: surface gravity waves, topographic effects

1. Introduction

In a recent paper (Choi 2022*a*), high-order strongly nonlinear (SNL) asymptotic models were considered for long surface gravity waves travelling on shallow water of constant depth h_0 assuming that the long wave parameter β is small, where β is defined as the ratio of h_0 to the characteristic wavelength λ_0 or $\beta := h_0/\lambda_0$. Depending on the choice of the order of approximation, it was shown that asymptotic long wave models for the

© The Author(s), 2026. Published by Cambridge University Press.

https://doi.org/10.1017/jfm.2026.11135 Published online by Cambridge University Press

depth-averaged horizontal velocity or the horizontal velocity at a fixed vertical level inside the fluid layer could be unstable for a range of wavenumbers or ill-posed in the sense that the growth rates of unstable short waves increase with the wavenumber (Matsuno 2016; Madsen & Fuhrman 2020). However, when the asymptotic long wave model is written for the bottom velocity, it was found linearly stable to all disturbances at any order of approximation. In addition, as β is the only small parameter in the expansion, it was shown that the SNL model reasonably well describes the dynamics of relatively large-amplitude waves (Choi 2022*a*). A similar expansion has also been applied to large-amplitude internal waves in a two-fluid system (Choi 2022*b*). This work extends the high-order SNL model to a variable bottom.

Wave deformation over variable bottom has been investigated by a number of researchers using various nonlinear long wave models. Kakutani (1971) generalised the Korteweg-de Vries (KdV) equation to the case of a variable bottom, and Johnson (1972) adopted a variable-coefficient KdV equation to study a solitary wave propagating over a shelf. Mei & Le Méhaute (1966), Peregrine (1967) and Madsen & Mei (1969) derived bi-directional weakly nonlinear (WNL) long wave models for a variable bottom that are equivalent to the Boussinesq model for a flat bottom. Dingemans (1994) compared some Boussinesq-type models with the laboratory measurements of periodic waves propagating over a submerged bar whose vertical cross-section is trapezoid shaped. Wei *et al.* (1995) derived a SNL Boussinesq model, applied to a solitary wave shoaling on slopes, and compared the computed results with those of a boundary element method for the fully nonlinear (FNL) problem developed by Grilli, Skouruo & Svendsen (1989). Madsen, Bingham & Liu (2002) presented a new Boussinesq-type model for highly nonlinear and dispersive waves over a variable bottom such that the linear dispersion relation is accurate for $kh_0 \leqslant 40$, where k denotes the characteristic wavenumber. Madsen, Fuhrman & Wang (2006) also generalised this model to cover rapidly varying bathymetry. Chazel, Lannes & Marche (2010) improved the Green–Naghdi (GN) equations (Green & Naghdi 1976) for the depth-averaged horizontal velocity valid to $O(\beta^2)$, proposed a new method of computation for it and compared the computed results with the experimental results of Dingemans (1994). Lannes & Marche (2015) also introduced a new type of GN equation over a varying bottom that has a mathematical structure suitable for numerical computations. Unfortunately, when they are extended to the next order, or to $O(\beta^4)$, the Boussinesq or GN equations become unstable and are no longer relevant for numerical computations (Matsuno 2016; Choi 2022*a*).

In this work, by generalising the high-order SNL models for a flat bottom, we derive those for a variable bottom written in terms of the bottom velocity by expanding systematically the velocity potential at the bottom in β^2. In addition to the fact that the use of the bottom velocity stabilises the asymptotic model, the high-order correction improves the linear dispersion relation, as shown in Choi (2022*a*, § 2), and, therefore, better describes the generation of relatively shorter waves that are often inaccurately modelled under the leading-order long wave approximation. To test the proposed high-order model for a variable bottom, we solve numerically the first- and second-order SNL models for two examples: (i) cnoidal waves propagating over a time-independent variable bottom, and (ii) the forced generation of solitary waves by a submerged bottom moving steadily with a transcritical speed, for which a succession of solitary waves is known to be generated and propagate ahead of the disturbance (Wu & Wu 1982; Wu 1987; Lee, Yates & Wu 1989; Grimshaw, Maleewong & Asavanant 2009). The numerical results of the SNL models are then compared with those of the WNL long wave model and the FNL computation using the boundary integral method developed by Baker, Meiron & Orszag (1982).

https://doi.org/10.1017/jfm.2026.11135 Published online by Cambridge University Press

This paper is organised as follows. Based on the formulation for nonlinear long waves using the bottom velocity in § 2, we present a systematic asymptotic expansion for the velocity potential and the vertical velocity in § 3, from which a high-order SNL model for a variable bottom is derived in § 4. The computed results of the proposed SNL model for the two examples mentioned previously are shown and discussed in § 5. Concluding remarks are given in § 6.

2. Basic formulation for nonlinear long waves

For water waves propagating in two horizontal dimensions, the free surface boundary conditions can be written (Zakharov 1968) as

$$\zeta_t = -\nabla\Phi\cdot\nabla\zeta + \big(1+|\nabla\zeta|^2\big)W, \quad \Phi_t = -\frac{1}{2}|\nabla\Phi|^2 - g\zeta + \frac{1}{2}\big(1+|\nabla\zeta|^2\big)W^2, \tag{2.1a,b}$$

where $\zeta(\boldsymbol{x},t)$ is the surface elevation, $\Phi(\boldsymbol{x},t)=\phi(\boldsymbol{x},z=\zeta,t)$ is the velocity potential evaluated at the free surface, W is the vertical velocity evaluated at the free surface defined by $W=\phi_z|_{z=\zeta}$ and g is the gravitational acceleration. Here $\boldsymbol{x}=(x,y)$, the subscripts t and z represent partial differentiations with respect to time t and the vertical coordinate z, respectively, and ∇ is the two-dimensional horizontal gradient given by $\nabla=(\partial/\partial x,\partial/\partial y)$.

There are several ways to write (2.1) as a closed system of two evolution equations for two dynamical variables. For example, one can express W in terms of ζ and Φ, as in the high-order spectral formulation (Dommermuth & Yue 1987; West *et al.* 1987; Craig & Sulem 1993), and then find a system for ζ and Φ, as commonly used for deep or intermediate water depth. Alternatively, for shallow water, one can find the expressions for Φ and W in terms of ζ and the bottom potential $\phi_b=\phi(\boldsymbol{x},z=-h,t)$ and write (2.1) as the evolution equations for these two variables (Choi 2022*a*).

As the first step to close (2.1), the velocity potential $\phi(\boldsymbol{x},z,t)$ and the vertical velocity $w(\boldsymbol{x},z,t)=\partial\phi/\partial z$ are expanded in Taylor series about the variable bottom $z=-h(\boldsymbol{x},t)$:

$$\phi(\boldsymbol{x},z,t)=\sum_{j=0}^{\infty}\left[\frac{(-1)^j(z+h)^{2j}}{(2j)!}\phi_{2j}+\frac{(-1)^j(z+h)^{2j+1}}{(2j+1)!}w_{2j}\right], \tag{2.2a}$$

$$w(\boldsymbol{x},z,t)=\sum_{j=0}^{\infty}\left[-\frac{(-1)^j(z+h)^{2j+1}}{(2j+1)!}\phi_{2j+2}+\frac{(-1)^j(z+h)^{2j}}{(2j)!}w_{2j}\right]. \tag{2.2b}$$

Here $\partial^2\phi/\partial z^2=-\nabla^2\phi$ has been used and $\phi_{2j}(\boldsymbol{x},t)$ and $w_{2j}(\boldsymbol{x},t)$ for $j=0,1,2,\cdots$ are defined, respectively, as

$$\phi_{2j}(\boldsymbol{x},t)=\big(\nabla^{2j}\phi\big)_{z=-h}, \quad w_{2j}(\boldsymbol{x},t)=\left(\nabla^{2j}\frac{\partial\phi}{\partial z}\right)_{z=-h}. \tag{2.3a,b}$$

Here we assume that the bottom is a known function in both space and time. In (2.3*a*) note that ϕ_{2j} for $j=0$ is the velocity potential at $z=-h$ so that $\phi_0=\phi_b(\boldsymbol{x},t)$.

When ϕ and w in (2.2) are evaluated at $z=\zeta$, the expressions for the free surface variable $\Phi(\boldsymbol{x},t)$ and $W(\boldsymbol{x},t)$ can be found as

https://doi.org/10.1017/jfm.2026.11135 Published online by Cambridge University Press

$$\Phi(\boldsymbol{x}, t) = \sum_{j=0}^{\infty}\left[\frac{(-1)^j \eta^{2j}}{(2j)!}\phi_{2j} + \frac{(-1)^j \eta^{2j+1}}{(2j+1)!}w_{2j}\right], \tag{2.4a}$$

$$W(\boldsymbol{x}, t) = \sum_{j=0}^{\infty}\left[-\frac{(-1)^j \eta^{2j+1}}{(2j+1)!}\phi_{2j+2} + \frac{(-1)^j \eta^{2j}}{(2j)!}w_{2j}\right], \tag{2.4b}$$

where η is the local depth defined by

$$\eta(\boldsymbol{x}, t) = h(\boldsymbol{x}, t) + \zeta(\boldsymbol{x}, t). \tag{2.5}$$

When the bottom is flat, as shown in Choi (2022*a*), (2.2) can be written, after imposing the bottom boundary condition given by $w_0 = 0$ and, therefore, $w_{2j} = 0$, as

$$\phi(\boldsymbol{x}, z, t) = \cos[(z+h)\nabla]\phi_b\ , \quad w(\boldsymbol{x}, z, t) = -\sin[(z+h)\nabla]\cdot\nabla\phi_b. \tag{2.6a,b}$$

Then, by substituting $z = \zeta$ into (2.6), Φ and W can be expressed, in terms of ζ and ϕ_b, as

$$\Phi = \cos(\eta\nabla)\phi_b, \quad W = -\sin(\eta\nabla)\cdot\nabla\phi_b. \tag{2.7a,b}$$

Substituting (2.7) into (2.1) yields formally a system of nonlinear evolution equations for ζ and ϕ_b although the cosine and sine functions in (2.7) need to be expanded in infinite series and, then, truncated for numerical evaluations. This has to be modified for a variable bottom and the derivation of the model will be presented in the following section.

3. Derivation of the long wave model for variable bottom

3.1. *Bottom boundary condition*

For the variable bottom located at $z = -h(x, t)$, the boundary condition given by

$$-(h_t + \nabla\phi\cdot\nabla h) = \frac{\partial\phi}{\partial z} \quad \text{at } z = -h(x, t) \tag{3.1}$$

can be rewritten, in terms of bottom variables ϕ_b and w_0 defined in (2.3), as

$$w_0 = -\frac{\dot{h}}{1+|\nabla h|^2}, \tag{3.2}$$

where $\dot{h}$ is defined as

$$\dot{h} = h_t + \nabla\phi_b\cdot\nabla h. \tag{3.3}$$

As mentioned previously, to write the system given by (2.1) as the evolution equations for ζ and ϕ_b, one needs to find the expressions for Φ and W in terms of these two variables. This can be achieved using (2.4) once ϕ_{2j} and w_{2j} are expressed in terms of ζ and ϕ_b, as described subsequently.

First, using the chain rule for differentiation, ϕ_2 and w_2 can be expressed as

$$\phi_2 = \left(\nabla^2\phi\right)_{z=-h} = \frac{1}{1+|\nabla h|^2}\left(\nabla^2\phi_0 + 2\nabla w_0\cdot\nabla h + w_0\nabla^2 h\right), \tag{3.4a}$$

$$w_2 = \left(\nabla^2 w\right)_{z=-h} = \frac{1}{1+|\nabla h|^2}\left(\nabla^2 w_0 - 2\nabla\phi_2\cdot\nabla h - \phi_2\nabla^2 h\right). \tag{3.4b}$$

Once the bottom boundary condition given by (3.2) is used for w_0, one has the expressions for ϕ_2 and w_2 in terms of ϕ_0. The general expressions for ϕ_{2j} and w_{2j} $(j = 1, 2, \cdots)$ can

https://doi.org/10.1017/jfm.2026.11135 Published online by Cambridge University Press

be found recursively as

$$\phi_{2j} = \left(\nabla^{2j}\phi\right)_{z=-h} = \frac{1}{1+|\nabla h|^2}\left(\nabla^2\phi_{2j-2} + 2\nabla w_{2j-2}\cdot\nabla h + w_{2j-2}\nabla^2 h\right), \tag{3.5a}$$

$$w_{2j} = \left(\nabla^{2j} w\right)_{z=-h} = \frac{1}{1+|\nabla h|^2}\left(\nabla^2 w_{2j-2} - 2\nabla\phi_{2j}\cdot\nabla h - \phi_{2j}\nabla^2 h\right). \tag{3.5b}$$

Then, substituting (3.4) and (3.5) into (2.4) and the resulting expressions for Φ and W into (2.1), one can find the closed system for the evolution equations for $\zeta(\boldsymbol{x}, t)$ and $\phi_b(\boldsymbol{x}, t)$. The resulting system (2.1) written in infinite series is exact, but needs to be truncated for practical applications. To find a long wave model that is asymptotically consistent, we need to expand ϕ_{2j} and w_{2j} in β^2, where $\beta = h_0/\lambda_0$ is the long wave parameter defined in § 1.

3.2. *Systematic asymptotic expansion*

We assume that ϕ_{2j} and w_{2j} ($j \geqslant 0$) in (3.5) can be expanded as

$$\phi_{2j} = \sum_{m=0}^{\infty}\phi_{2j,2m}, \quad w_{2j} = \sum_{m=0}^{\infty} w_{2j,2m}. \tag{3.6a,b}$$

In (3.6), $\phi_{0,2m}$ is given by

$$\phi_{0,0} = \phi_b, \quad \phi_{0,2m} = 0 \quad \text{for} \quad m \geqslant 1, \tag{3.7a,b}$$

while $w_{0,2m}$ are given, from (3.2), by

$$w_{0,2m} = (-1)^{m+1}\,|\nabla h|^{2m}\,\dot{h} \quad \text{for} \quad m \geqslant 0, \tag{3.7c}$$

where we have used the fact that

$$(1+|\nabla h|^2)^{-1} = \sum_{m=0}^{\infty}(-1)^m\,|\nabla h|^{2m}, \tag{3.8}$$

with $|\nabla h|^2 = O(\beta^2)$. On the other hand, for $j \geqslant 1$, $\phi_{2j,2m}$ and $w_{2j,2m}$ are given, from (3.5), by

$$\phi_{2j,0} = \nabla^2\phi_{2j-2,0}, \tag{3.9a}$$

$$\begin{aligned}\phi_{2j,2m} = {}& \sum_{l=0}^{m}(-1)^l|\nabla h|^{2l}\,\nabla^2\phi_{2j-2,2(m-l)} \\ & + \sum_{l=0}^{m-1}(-1)^l|\nabla h|^{2l}\left(2\nabla w_{2j-2,2(m-l-1)}\cdot\nabla h + w_{2j-2,2(m-l-1)}\nabla^2 h\right) \quad \text{for } m \geqslant 1,\end{aligned} \tag{3.9b}$$

$$\begin{aligned}w_{2j,2m} = {}& \sum_{l=0}^{m}(-1)^l|\nabla h|^{2l}\left(\nabla^2 w_{2j-2,2(m-l)} - 2\nabla\phi_{2j,2(m-l)}\cdot\nabla h - \phi_{2j,2(m-l)}\nabla^2 h\right) \\ & \text{for } m \geqslant 0.\end{aligned} \tag{3.9c}$$

Note that $\phi_{2j,2m}/\phi_b = O(\beta^{2(j+m)})$ and $w_{2j,2m}/|\nabla\phi_b| = O(\beta^{2(j+m)+1})$ as $|\nabla h|^{2m} = O(\beta^{2m})$ and $|w/\nabla\phi| = O(\beta)$ for long waves. Although no small parameter is explicitly introduced, one can see that ϕ_{2j} and w_{2j} are expanded in β^2 in (3.6).

https://doi.org/10.1017/jfm.2026.11135 Published online by Cambridge University Press

3.3. *Expansion for Φ and W in terms of ζ and ϕ_b*

After substituting (3.6) with (3.7) and (3.9) into (2.4) and collecting terms at $O(\beta^2)$, Φ and W can be expanded as

$$\Phi = \sum_{m=0}^{\infty} \Phi_{2m}, \quad W = \sum_{m=0}^{\infty} W_{2m}, \tag{3.10a,b}$$

where Φ_{2m} and W_{2m} are given by

$$\Phi_0 = \phi_b, \tag{3.11a}$$

$$\Phi_{2m} = \sum_{n=0}^{m-1} (-1)^n \left[-\frac{\eta^{2n+2}}{(2n+2)!} \phi_{2n+2,2(m-n-1)} + \frac{\eta^{2n+1}}{(2n+1)!} w_{2n,2(m-n-1)} \right] \quad \text{for } m \geqslant 1, \tag{3.11b}$$

$$W_{2m} = \sum_{n=0}^{m} (-1)^n \left[-\frac{\eta^{2n+1}}{(2n+1)!} \phi_{2n+2,2(m-n)} + \frac{\eta^{2n}}{(2n)!} w_{2n,2(m-n)} \right] \quad \text{for } m \geqslant 0, \tag{3.11c}$$

where $\phi_{0,2m} = 0$ for $m \geqslant 1$ has been imposed.

Note that both Φ_{2m} and W_{2m} explicitly depend only on ζ and ϕ_b. Assuming that $\eta\nabla = O(h_0/\lambda_0) = O(\beta) \ll 1$ with $\zeta/h = O(a_0/h_0) = O(\alpha) = O(1)$, one can notice that $\Phi_{2m}/\Phi = O(\beta^{2m})$ and $W_{2m}/|\nabla\Phi| = O(\beta^{2m+1})$ for $m \geqslant 0$. Here α is the nonlinearity parameter defined by the ratio of the wave amplitude a_0 to the water depth h_0, namely $\alpha := a_0/h_0$, and note that no assumption on the magnitude of α is made. Therefore, as long as β remains small, the amplitude a_0 can be comparable to h_0. Of course, the assumption of $\beta \ll 1$ is no longer valid for short waves, for which a high-order correction is necessary.

4. High-order long wave model for the bottom potential

4.1. *System of nonlinear evolution equations*

By substituting (3.10) into (2.1), the nonlinear evolution equations for ζ and ϕ_b can be obtained as

$$\zeta_t = \sum_{m=0}^{\infty} Q_{2m}(\zeta, \phi_b), \quad \Phi_t = \sum_{m=0}^{\infty} R_{2m}(\zeta, \phi_b), \tag{4.1a,b}$$

where Φ is given, in terms of ζ and ϕ_b, by (3.10a). In (4.1), Q_{2m} ($m \geqslant 0$) are given by

$$Q_0 = -\nabla\zeta \cdot \nabla\Phi_0 + W_0, \quad Q_{2m} = -\nabla\zeta \cdot \nabla\Phi_{2m} + W_{2m} + |\nabla\zeta|^2 W_{2(m-1)} \quad \text{for } m \geqslant 1, \tag{4.2a,b}$$

while R_{2m} ($m \geqslant 0$) are given by

$$R_0 = -g\zeta - \frac{1}{2}|\nabla\Phi_0|^2, \quad R_2 = -\nabla\Phi_0 \cdot \nabla\Phi_2 + \frac{1}{2}{W_0}^2, \tag{4.3a,b}$$

$$R_{2m} = -\frac{1}{2}\sum_{j=0}^{m} \nabla\Phi_{2j} \cdot \nabla\Phi_{2(m-j)} + \frac{1}{2}\sum_{j=0}^{m-1} W_{2j} W_{2(m-j-1)} + \frac{1}{2}|\nabla\zeta|^2 \sum_{j=0}^{m-2} W_{2j} W_{2(m-j-2)} \quad \text{for } m \geqslant 2. \tag{4.3c}$$

Note that both Q_{2m} and R_{2m} are $O(\beta^{2m})$ as $\Phi_{2m} = O(W_{2m}) = O(\beta^{2m})$.

https://doi.org/10.1017/jfm.2026.11135 Published online by Cambridge University Press

Similarly to the case of a flat bottom, the evolution equation for ζ given by (4.1a) can be written in terms of the depth-averaged velocity $\overline{\boldsymbol{u}}$ defined by

$$\eta\overline{\boldsymbol{u}} = \int_{-h}^{\zeta} \nabla\phi \, \mathrm{d}z, \tag{4.4}$$

whose divergence can be shown, after some manipulation using (2.2a), (2.4) and (3.5), to be

$$\nabla\cdot(\eta\overline{\boldsymbol{u}}) = \nabla\Phi\cdot\nabla\zeta - (1+|\nabla\zeta|^2)W - h_t = -\sum_{m=0}^{\infty} Q_{2m} - h_t. \tag{4.5}$$

Then, (2.1a) can be reduced to

$$\zeta_t + \nabla\cdot(\eta\overline{\boldsymbol{u}}) = -h_t, \tag{4.6}$$

which implies conservation of mass when $h_t = 0$.

4.2. *Truncated systems*

For practical applications, the system (4.1) needs to be truncated, after replacing the upper limit of the summation by M, to

$$\zeta_t = \sum_{m=0}^{M} Q_{2m}(\zeta, \phi_b), \quad \Phi_t = \sum_{m=0}^{M} R_{2m}(\zeta, \phi_b). \tag{4.7a,b}$$

The truncated system (4.7) is valid to $O(\beta^{2M})$, which will be hereinafter referred to as the Mth-order system.

4.2.1. *Zeroth-order model*

Under the zeroth-order ($M = 0$) approximation, the leading-order terms in (4.7) can be obtained as $\zeta_t = Q_0$ and $\Phi_{0t} = R_0$ or

$$\zeta_t + \nabla\cdot(\eta\nabla\phi_b) = -h_t, \quad \phi_{bt} + g\zeta + \frac{1}{2}|\nabla\phi_b|^2 = 0, \tag{4.8a,b}$$

which is the (non-dispersive) shallow water equations and neglects any terms of $O(\beta^2)$ or smaller.

4.2.2. *First-order model*

Under the first-order ($M = 1$) approximation, the system correct to $O(\beta^2)$ can be found as

$$\zeta_t = Q_0 + Q_2, \quad (\Phi_0 + \Phi_2)_t = R_0 + R_2, \tag{4.9a,b}$$

which can be written explicitly, for Φ_{2m}, Q_{2m} and R_{2m} ($m = 0, 1$), respectively, as

$$\zeta_t + \nabla\cdot\left[\left(\eta - \frac{\eta^3}{3!}\nabla^2\right)\nabla\phi_b - \frac{\eta^2}{2}\nabla\dot{h} - \left(\frac{\eta^2}{2}\nabla^2\phi_b + \eta\dot{h}\right)\nabla h\right] = -h_t, \tag{4.10a}$$

$$\left[\left(1 - \frac{\eta^2}{2!}\nabla^2\right)\phi_b - \eta\dot{h}\right]_t + g\zeta + \frac{1}{2}\nabla\phi_b\cdot\nabla\phi_b = \nabla\cdot\left(\frac{\eta^2}{2!}\nabla^2\phi_b\nabla\phi_b + \eta\dot{h}\nabla\phi_b\right) + \frac{1}{2}\dot{h}^2, \tag{4.10b}$$

which is valid to $O(\beta^2)$.

When h is independent of time t so that $h_t = 0$ and $\dot{h} = \nabla\phi_b\cdot\nabla h$, this system can be reduced to that derived by Wei *et al.* (1995) for the bottom velocity potential.

https://doi.org/10.1017/jfm.2026.11135 Published online by Cambridge University Press

After taking the horizontal gradient, the first-order system (4.10) can be written, in terms of $\boldsymbol{v} = \nabla\phi_b$, as

$$\zeta_t + \nabla\cdot\left[\left(\eta - \frac{\eta^3}{3!}\nabla^2\right)\boldsymbol{v} - \frac{\eta^2}{2}\nabla\dot{h} - \left(\frac{\eta^2}{2}\nabla\cdot\boldsymbol{v} + \eta\dot{h}\right)\nabla h\right] = -h_t, \tag{4.11a}$$

$$\left[\boldsymbol{v} - \nabla\left(\frac{\eta^2}{2!}\nabla\cdot\boldsymbol{v} + \eta\dot{h}\right)\right]_t + \nabla\left(g\zeta + \frac{1}{2}\boldsymbol{v}\cdot\boldsymbol{v}\right) = \nabla\left[\nabla\cdot\left\{\frac{\eta^2}{2!}(\nabla\cdot\boldsymbol{v})\boldsymbol{v} + \eta\dot{h}\boldsymbol{v}\right\} + \frac{1}{2}\dot{h}^2\right], \tag{4.11b}$$

where $\dot{h} = h_t + \boldsymbol{v}\cdot\nabla h$ and $\boldsymbol{v}$ is referred to as the bottom velocity. Note that $\boldsymbol{v}$ is a tangential velocity at the bottom when it is divided by $(1+|\nabla h|^2)^{1/2}$.

For WNL waves of $\zeta/h = O(\beta^2)$, or $\alpha = O(\beta^2)$, the first-order system given by (4.11) can be further simplified to the following WNL model:

$$\zeta_t + \nabla\cdot\left[\eta\boldsymbol{v} - \nabla\left(\frac{h^3}{3!}\nabla\cdot\boldsymbol{v} + \frac{h^2}{2}\dot{h}\right)\right] = -h_t, \tag{4.12a}$$

$$\left[\boldsymbol{v} - \nabla\left(\frac{h^2}{2!}\nabla\cdot\boldsymbol{v} + h\dot{h}\right)\right]_t + \nabla\left(g\zeta + \frac{1}{2}\boldsymbol{v}\cdot\boldsymbol{v}\right) = \nabla\left[\nabla\cdot(hh_t\boldsymbol{v}) + \frac{1}{2}h_t(h_t + 2\boldsymbol{v}\cdot\nabla h)\right]. \tag{4.12b}$$

Here we have assumed that $|\nabla h| = O(h_t) = O(\beta)$ and have used the fact that $\nabla(\nabla\cdot\boldsymbol{v}) = \nabla^2\boldsymbol{v}$ with $\nabla\times\boldsymbol{v} = \nabla\times\nabla\phi_b = 0$.

By comparing (4.11a) with (4.6), one can see that the depth-averaged velocity can be expressed, in terms of $\boldsymbol{v}$, as

$$\overline{\boldsymbol{u}} = \left(1 - \frac{\eta^2}{3!}\nabla^2\right)\boldsymbol{v} - \frac{\eta}{2}\nabla\dot{h} - \left(\frac{\eta}{2}\nabla\cdot\boldsymbol{v} + \dot{h}\right)\nabla h + O(\beta^4), \tag{4.13}$$

which can be inverted, under the same order of approximation, to

$$\boldsymbol{v} = \left(1 + \frac{\eta^2}{3!}\nabla^2\right)\overline{\boldsymbol{u}} + \frac{\eta}{2}\nabla\overline{\dot{h}} + \left(\frac{\eta}{2}\nabla\cdot\overline{\boldsymbol{u}} + \overline{\dot{h}}\right)\nabla h + O(\beta^4), \tag{4.14}$$

where $\overline{\dot{h}}$ is defined by

$$\overline{\dot{h}} = h_t + \overline{\boldsymbol{u}}\cdot\nabla h. \tag{4.15}$$

The same result can be obtained from the definition of $\overline{u}$ given by (4.4) with (2.2a) and (3.10a), as shown in Appendix B. Then, by substituting (4.14) into (4.11) and neglecting terms higher than $O(\beta^2)$, one can find the first-order system for the depth-averaged velocity given, in conservative form, by

$$\left[\overline{\boldsymbol{u}} - \frac{1}{\eta}\nabla\left(\frac{\eta^3}{3}\nabla\cdot\overline{\boldsymbol{u}} + \frac{\eta^2}{2}\overline{\dot{h}}\right) + \left(\frac{\eta}{2}\nabla\cdot\overline{\boldsymbol{u}} + \overline{\dot{h}}\right)\nabla h\right]_t + \nabla\left(g\zeta + \frac{1}{2}\overline{\boldsymbol{u}}\cdot\overline{\boldsymbol{u}}\right)$$
$$= \nabla\left[\frac{1}{2}\left(\eta\nabla\cdot\overline{\boldsymbol{u}} + \overline{\dot{h}}\right)^2 + \frac{\overline{\boldsymbol{u}}}{\eta}\cdot\nabla\left(\frac{\eta^3}{3}\nabla\cdot\overline{\boldsymbol{u}} + \frac{\eta^2}{2}\overline{\dot{h}}\right) - \overline{\boldsymbol{u}}\cdot\left(\frac{\eta}{2}\nabla\cdot\overline{\boldsymbol{u}} + \overline{\dot{h}}\right)\nabla h\right]. \tag{4.16}$$

Here we have used $\nabla(\nabla\cdot\overline{\boldsymbol{u}}) = \nabla^2\overline{\boldsymbol{u}} + O(\beta^2)$ from the fact that

$$\nabla\times\overline{\boldsymbol{u}} = -\nabla\eta\times\left(\frac{\eta}{3}\nabla^2\overline{\boldsymbol{u}} + \frac{1}{2}\nabla\overline{\dot{h}}\right) + \nabla h\times\nabla\left(\frac{\eta}{2}\nabla\cdot\overline{\boldsymbol{u}} + \overline{\dot{h}}\right) + O(\beta^4) = O(\beta^2), \tag{4.17}$$

https://doi.org/10.1017/jfm.2026.11135 Published online by Cambridge University Press

which is obtained by taking the curl of (4.14) with $\nabla \times \boldsymbol{v} = \nabla \times \nabla \phi_b = 0$.

Using $\nabla(\overline{\boldsymbol{u}} \cdot \overline{\boldsymbol{u}}) = 2\overline{\boldsymbol{u}} \cdot \nabla \overline{\boldsymbol{u}} + 2\overline{\boldsymbol{u}} \times (\nabla \times \overline{\boldsymbol{u}})$ with (4.17), one can rewrite (4.16), after some lengthy manipulation, as

$$\overline{\boldsymbol{u}}_t + \overline{\boldsymbol{u}} \cdot \nabla \overline{\boldsymbol{u}} + g\nabla\zeta = \frac{1}{\eta}\nabla\left(\frac{\eta^3}{3}G + \frac{\eta^2}{2}F\right) - \left(\frac{\eta}{2}G + F\right)\nabla h, \tag{4.18}$$

where G and F are defined by

$$G = \nabla \cdot \overline{\boldsymbol{u}}_t + \overline{\boldsymbol{u}} \cdot \nabla(\nabla \cdot \overline{\boldsymbol{u}}) - (\nabla \cdot \overline{\boldsymbol{u}})^2, \quad F = (\partial_t + \overline{\boldsymbol{u}} \cdot \nabla)\overline{\dot{h}}. \tag{4.19a,b}$$

Equation (4.18) along with (4.6) yields the GN equations for a variable bottom correct to $O(\beta^2)$.

4.2.3. *Second-order model*

The second-order ($M = 2$) system for ζ and $\boldsymbol{v}$ that is correct to $O(\beta^4)$ can be found, from (A3), (A5) and (A6) for Φ_{2m}, R_{2m} and Q_{2m} ($m = 0, 1, 2$), respectively, as

$$\zeta_t = Q_0 + Q_2 + Q_4, \quad (\Phi_0 + \Phi_2 + \Phi_4)_t = R_0 + R_2 + R_4. \tag{4.20a,b}$$

Alternatively, by taking the gradient of (4.20*b*), one can find the system for ζ and $\boldsymbol{v}$ as

$$\zeta_t + \nabla \cdot \left[\left\{\eta - \frac{\eta^3}{3!}\nabla^2 + \frac{\eta^5}{5!}(\nabla^2)^2\right\}\boldsymbol{v} - \frac{\eta^2}{2!}\nabla\dot{h} - \left(\frac{\eta^2}{2!}\nabla \cdot \boldsymbol{v} + \eta\dot{h}\right)\nabla h + \frac{\eta^4}{4!}\nabla\Omega + \frac{\eta^3}{3!}\nabla\Pi + \frac{\eta^2}{2!}\nabla\left(|\nabla h|^2\dot{h}\right) + \Phi_4\nabla h\right] = -h_t, \tag{4.21a}$$

$$\left[\boldsymbol{v} - \nabla\left(\frac{\eta^2}{2!}\nabla \cdot \boldsymbol{v} + \eta\dot{h}\right) + \nabla\Phi_4\right]_t + \nabla\left(g\zeta + \frac{1}{2}\boldsymbol{v} \cdot \boldsymbol{v}\right)$$
$$= \nabla\left[\nabla \cdot \left\{\frac{\eta^2}{2!}(\nabla \cdot \boldsymbol{v})\boldsymbol{v} + \eta\boldsymbol{v}\dot{h}\right\} + \frac{1}{2}\dot{h}^2\right]$$
$$- \nabla\left[\boldsymbol{v} \cdot \nabla\Phi_4 + \frac{1}{2}\left|\nabla\left(\frac{\eta^2}{2!}\nabla \cdot \boldsymbol{v} + \eta\dot{h}\right)\right|^2 + W_2(\eta\nabla \cdot \boldsymbol{v} + \dot{h}) - \frac{1}{2}|\nabla\zeta|^2(\eta\nabla \cdot \boldsymbol{v} + \dot{h})^2\right], \tag{4.21b}$$

where W_2 and Φ_4 are given by

$$W_2 = \frac{\eta^3}{3!}\nabla \cdot \nabla^2\boldsymbol{v} + \frac{\eta^2}{2!}\Omega + \eta\Pi + |\nabla h|^2\dot{h}, \tag{4.22a}$$

$$\Phi_4 = \frac{\eta^4}{4!}\nabla^2\nabla \cdot \boldsymbol{v} + \frac{\eta^3}{3!}\Omega + \frac{\eta^2}{2!}\Pi + \eta|\nabla h|^2\dot{h}, \tag{4.22b}$$

with Ω and Π defined by

$$\Omega = \nabla^2\dot{h} + 2\nabla^2\boldsymbol{v} \cdot \nabla h + (\nabla \cdot \boldsymbol{v})\nabla^2 h, \quad \Pi = |\nabla h|^2\nabla \cdot \boldsymbol{v} + 2\nabla\dot{h} \cdot \nabla h + \dot{h}\nabla^2 h. \tag{4.23a,b}$$

In the absence of variable bottom topography ($h_t = |\nabla h| = 0$), the second-order system (4.21) can be reduced to

$$\zeta_t + \nabla \cdot \left[\left\{\eta - \frac{\eta^3}{3!}\nabla^2 + \frac{\eta^5}{5!}(\nabla^2)^2\right\}\boldsymbol{v}\right] = 0, \tag{4.24a}$$

https://doi.org/10.1017/jfm.2026.11135 Published online by Cambridge University Press

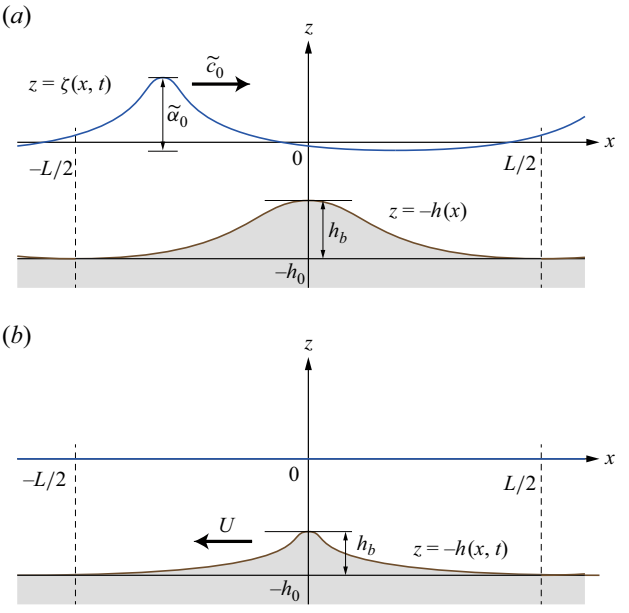


Figure 1. Schematic views of initial states for two numerical examples. (*a*) Example 1: long waves propagating over a time-independent variable bottom $z = -h(x)$. (*b*) Example 2: the forced generation of solitary waves by a bottom topography $z = -h(x, t)$ moving to the left steadily with a transcritical speed. The blue line —— represents the water surface $z = \zeta(x, t)$ and the brown line —— the bottom topography $z = -h(x, t)$.

$$\left[\boldsymbol{v} - \boldsymbol{\nabla}\left(\frac{\eta^2}{2!}\boldsymbol{\nabla}\cdot\boldsymbol{v} - \frac{\eta^4}{4!}\boldsymbol{\nabla}\cdot\nabla^2\boldsymbol{v}\right)\right]_t + \boldsymbol{\nabla}\left(g\zeta + \frac{1}{2}\boldsymbol{v}\cdot\boldsymbol{v}\right)$$
$$= \boldsymbol{\nabla}\left[\boldsymbol{\nabla}\cdot\left(\frac{\eta^4}{4!}\boldsymbol{v}\nabla^2\boldsymbol{\nabla}\cdot\boldsymbol{v} + \frac{\eta^4}{16}\boldsymbol{\nabla}(\boldsymbol{\nabla}\cdot\boldsymbol{v})^2\right)\right]. \tag{4.24b}$$

Note that the original form on the right-hand side of (4.24*b*) in Choi (2022*a*) contained an error, which was corrected in Choi (2022*c*). When linearised, both (4.11) and (4.24) have the real dispersion relation for any wavenumber and are therefore neutrally stable in the absence of bottom topography.

5. Numerical examples

This section shows some computed results for two examples: (i) example : long waves propagating over a time-independent variable bottom $z = -h(x)$; and (ii) example 2: the forced generation of solitary waves by a bottom topography $z = -h(x, t)$ moving to the left steadily with a transcritical speed, as shown in figures 1(*a*) and 1(*b*), respectively. The flow is two-dimensional in the vertical cross-section along the propagation direction of waves, and each variable is one-dimensional in space, such as $\zeta = \zeta(x, t)$, $\phi_{bx} = v = v(x, t)$ and $h = h(x, t)$.

For numerical computation, each variable is non-dimensionalised with the length scale h_0 and the time scale $\sqrt{h_0/g}$ as

$$(x_*, z_*, t_*, L_*, \zeta_*, h_*, \eta_*, v_*) = \left(\frac{x}{h_0}, \frac{z}{h_0}, \frac{t}{\sqrt{h_0/g}}, \frac{L}{h_0}, \frac{\zeta}{h_0}, \frac{h}{h_0}, \frac{\eta}{h_0}, \frac{v}{\sqrt{gh_0}}\right). \tag{5.1}$$

https://doi.org/10.1017/jfm.2026.11135 Published online by Cambridge University Press

Henceforth, the asterisks for dimensionless variables will be omitted for brevity. For this one-dimensional system in space, the first-order SNL model (4.11) can be rewritten in dimensionless form as

$$\zeta_t = \left\{ -(\eta v - \frac{\eta^3}{3!} v_{xx}) + \frac{\eta^2}{2!}(\dot{h}_x + v_x h_x) + \eta \dot{h} h_x \right\}_x - h_t, \tag{5.2a}$$

$$\left[v - \partial_x \left(\frac{\eta^2}{2} v_x + \eta \dot{h} \right) \right]_t = \left\{ -\zeta - \frac{1}{2} v^2 + \left(\frac{\eta^2}{2} v v_x + \eta \dot{h} v \right)_x + \frac{1}{2} \dot{h}^2 \right\}_x, \tag{5.2b}$$

and the second-order SNL model (4.21) as

$$\begin{aligned} \zeta_t = \Bigg\{ & -(\eta v - \frac{\eta^3}{3!} v_{xx} + \frac{\eta^5}{5!} v_{xxxx}) + \frac{\eta^2}{2!}(\dot{h}_x + v_x h_x) + \eta \dot{h} h_x \\ & - \frac{\eta^4}{4!} \Omega_x - \frac{\eta^3}{3!} \Pi_x - \frac{\eta^2}{2!} ({h_x}^2 \dot{h})_x - \Phi_4 h_x \Bigg\}_x - h_t, \end{aligned} \tag{5.3a}$$

$$\begin{aligned} \left[v - \left(\frac{\eta^2}{2!} v_x + \eta \dot{h} \right)_x + \Phi_{4x} \right]_t = \Bigg[& -\zeta - \frac{1}{2} v^2 + \left(\frac{\eta^2}{2!} v_x v + \eta v \dot{h} \right)_x + \frac{1}{2} \dot{h}^2 \\ & - v \Phi_{4x} - \frac{1}{2} \left\{ \left(\frac{\eta^2}{2!} v_x + \eta \dot{h} \right)_x \right\}^2 - W_2 (\eta v_x + \dot{h}) + \frac{1}{2} {\zeta_x}^2 (\eta v_x + \dot{h})^2 \Bigg]_x, \end{aligned} \tag{5.3b}$$

where

$$\left. \begin{aligned} & \Omega = \dot{h}_{xx} + 2 v_{xx} h_x + v_x h_{xx}, \quad \Pi = {h_x}^2 v_x + 2 \dot{h}_x h_x + \dot{h} h_{xx} \\ & \Phi_4 = \frac{\eta^4}{4!} v_{xxx} + \frac{\eta^3}{3!} \Omega + \frac{\eta^2}{2!} \Pi + \eta {h_x}^2 \dot{h}, \quad W_2 = \frac{\eta^3}{3!} v_{xxx} + \frac{\eta^2}{2!} \Omega + \eta \Pi + {h_x}^2 \dot{h} \end{aligned} \right\}. \tag{5.3c}$$

After assuming the amplitude parameter $\alpha \ll 1$ with $\alpha = O(\beta^2)$, $h - h_0 = O(\alpha)$, $h_x = O(h_t) = O(\alpha\beta)$, and neglecting terms higher than $O(\alpha\beta^3, \alpha^2\beta)$, the WNL long wave model (4.12) for the one-dimensional system in space becomes

$$\zeta_t = \left[-\eta v + \left(\frac{h^3}{3!} v \right)_{xx} \right]_x - h_t, \quad \left[v - \left(\frac{h^2}{2!} v \right)_{xx} \right]_t = \left(-\zeta - \frac{1}{2} v^2 \right)_x. \tag{5.4a,b}$$

After rearranging dispersive terms for $h_t = 0$, it can be shown that (5.4) is the WNL system of Mei & Le Méhaute (1966).

Suppose that the flow domain and the bottom topography are periodic in space as $\zeta(x, t) = \zeta(x + L, t)$, $v(x, t) = v(x + L, t)$ and $h(x, t) = h(x + L, t)$. We numerically solve the SNL models (5.2) and (5.3) and the WNL model (5.4) in the domain $-L/2 \leqslant x \leqslant L/2$ using a pseudo-spectral method with periodic boundary conditions, similarly to the previous work (Choi 2022*a*, § 6.2) for a flat bottom. The computed results are compared with the FNL computation based on the boundary integral method developed by Baker *et al.* (1982), which is summarised in Appendix D.

5.1. *The computational method of long wave models*

For the spectral approximation of ζ and v in the first- and second-order SNL models (5.2) and (5.3) and the WNL model (5.4), the computational domain $-L/2 < x < L/2$ is transformed into $-\pi < \xi < \pi$, namely

$$-\frac{L}{2} < x < \frac{L}{2} \quad \Leftrightarrow \quad -\pi < \xi < \pi \quad \text{with } x = \frac{L}{2\pi} \xi, \tag{5.5}$$

https://doi.org/10.1017/jfm.2026.11135 Published online by Cambridge University Press

and is divided at equal intervals as

$$x_j = -\frac{L}{2} + j\Delta x \quad \Leftrightarrow \quad \xi_j = -\pi + j\Delta\xi \quad \text{with } \Delta x = \frac{L}{N}, \quad \Delta\xi = \frac{2\pi}{N} \quad (j = 0, 1, \cdots, N). \tag{5.6}$$

Then ζ and v at $x = x_j = (L/(2\pi))\xi_j$ can be approximated, respectively, as

$$\zeta_j(t) := \zeta(x_j, t) = \sum_{k=-\frac{N}{2}}^{\frac{N}{2}-1} \check{\zeta}_k(t) \mathrm{e}^{ik\xi_j} \quad \text{with} \quad \check{\zeta}_k(t) = \frac{1}{N}\sum_{j=0}^{N-1} \zeta_j(t)\mathrm{e}^{-ik\xi_j}, \tag{5.7a}$$

$$v_j(t) := v(x_j, t) = \sum_{k=-\frac{N}{2}}^{\frac{N}{2}-1} \check{v}_k(t) \mathrm{e}^{ik\xi_j} \quad \text{with} \quad \check{v}_k(t) = \frac{1}{N}\sum_{j=0}^{N-1} v_j(t)\mathrm{e}^{-ik\xi_j}. \tag{5.7b}$$

Here the Fourier coefficients $\check{\gamma}_k = \check{\zeta}_k$ or $\check{v}_k$ are numerically obtained using a fast Fourier transform. In addition, in order to reduce aliasing errors due to approximation of nonlinear terms using the finite Fourier series, the Fourier coefficients $\check{\gamma}_k = \check{\zeta}_k$ or $\check{v}_k$ are filtered as

$$\check{\gamma}_k = \begin{cases} \check{\gamma}_k & \text{for } |k| \leqslant \dfrac{N}{2} - N_{filter}, \\ 0 & \text{for } |k| > \dfrac{N}{2} - N_{filter}. \end{cases} \tag{5.8}$$

The evolution equations in (5.2), (5.3) and (5.4) are integrated in time using the fourth-order Runge–Kutta scheme. Then, in order to determine v at a new time step, we apply the same iterative scheme as in the previous work (Choi 2022*a*, (6.14)) to the second equations (5.2*b*), (5.3*b*) and (5.4*b*). For the second-order SNL model, we solve (5.3*b*) to obtain Ψ defined by

$$\Psi := v - \left(\frac{\eta^2}{2!}v_x + \eta v h_x\right)_x + \Phi_{4x}, \tag{5.9}$$

and invert this to find v at a new time step using the following iterative scheme:

$$\left(1 - \frac{{\eta_{\max}}^2}{2!}\frac{\partial^2}{\partial x^2} + \frac{{\eta_{\max}}^4}{4!}\frac{\partial^4}{\partial x^4}\right) v^{(\mu+1)} = \Psi^{(\mu)} + \left\{\left(\frac{\eta^2}{2!} - \frac{{\eta_{\max}}^2}{2!}\right) v_x^{(\mu)} - \left(\frac{\eta^4}{4!} - \frac{{\eta_{\max}}^4}{4!}\right) v_{xxx}^{(\mu)} + \eta v^{(\mu)} h_x - \frac{\eta^3}{3!}\Omega^{(\mu)} - \frac{\eta^2}{2!}\Pi^{(\mu)} - \eta v^{(\mu)} {h_x}^3\right\}_x \quad (\mu = 0, 1, \cdots). \tag{5.10}$$

Here μ denotes the iteration number and $\eta_{\max} = \max_{0\leqslant j\leqslant N}\eta(x_j, t)$ is a numerical parameter to accelerate the convergence rate (see Choi 2022*a*, Appendix C). Note that Ψ in (5.9) corresponds to the inside of the bracket on the left-hand side of (5.3*b*). The stopping condition of this iteration (5.10) was set using the residual $r^{(\mu)}(t)$ as

$$r^{(\mu)}(t) := \max_{0\leqslant j\leqslant N} |v^{(\mu)}(x_j, t) - v^{(\mu-1)}(x_j, t)| < 10^{-9}. \tag{5.11}$$

In the case of a variable bottom, the convergence rate of this iterative scheme (5.10) depends sensitively on the initial guess $v^{(0)}$. We improve the convergence of (5.10) by adopting a solution of the finite difference approximation of (5.9) as the initial guess $v^{(0)}$ (see Appendix C). Similarly, we can obtain v at a new time step in (5.2*b*) of the first-order SNL model and (5.4*b*) of the WNL model.

https://doi.org/10.1017/jfm.2026.11135 Published online by Cambridge University Press

5.2. *Example 1: long waves propagating over a time-independent variable bottom ($h_t = 0$)*

The initial state of this example is schematically depicted in figure 1(*a*). The initial wave and the bottom topography are set as follows. First, the initial wave profile $z = \zeta(x, t = 0)$ is the cnoidal wave solution of the KdV equation given by

$$\zeta(x, t = 0) = -\tilde{\alpha}_0\, B(\ell) + \tilde{\alpha}_0\, \mathrm{cn}^2 \left\{ \frac{\sqrt{3\tilde{\alpha}_0}}{2\ell}(x - x_0) \,\middle|\, \ell \right\}, \tag{5.12}$$

with

$$B(\ell) := 1 - \frac{1}{\ell^2} + \frac{1}{\ell^2}\frac{E(\ell)}{K(\ell)}, \tag{5.13}$$

where ℓ denotes the modulus of the cnoidal function, $K(\ell)$ and $E(\ell)$ are the complete elliptic integrals of the first and second kind, respectively, and $\tilde{\alpha}_0 = H_0/h_0$ is the dimensionless height of the initial wave. The wave crest is located at $x = x_0$. When the wavelength L and the wave height $\tilde{\alpha}_0$ are given, the modulus ℓ can be determined by

$$\ell \cdot K(\ell) = \frac{\sqrt{3\tilde{\alpha}_0}}{4} L. \tag{5.14}$$

The phase speed $\tilde{c}_0$ of the initial cnoidal wave in (5.12) is given by

$$\tilde{c}_0 = 1 + \frac{1}{2}\tilde{\alpha}_0 \left\{ 2 - \frac{1}{\ell^2} - 3B(\ell) \right\}, \tag{5.15}$$

where $\tilde{c}_0$ is scaled by $\sqrt{gh_0}$. Next, the time-independent bottom topography $z = -h(x)$ is set using the cnoidal function as

$$h(x) = 1 - h_b\, \mathrm{cn}^6 \left\{ \frac{2}{L} K(\ell_b) x \,\middle|\, \ell_b \right\}, \tag{5.16}$$

where h_b is the height of the topography, as shown in figure 1(*a*), and the modulus ℓ_b is related to the nome q_{ℓ_b} by

$$q_{\ell_b} = \exp\left(-\pi \frac{K'(\ell_b)}{K(\ell_b)} \right) \quad \text{with } K'(\ell_b) = K(\ell_b') = K(\sqrt{1 - {\ell_b}^2}). \tag{5.17}$$

Figures 2 and 3 show some computed results of the first- and second-order SNL long wave models (5.2) and (5.3) and the WNL long wave model (5.4) with $L = 60$, $x_0 = -20$ in (5.12) and $h_b = 0.75$ and $q_{\ell_b} = 0.01$ in (5.16). The results are compared with the FNL computation. Figure 2(*d*) shows the shape of the bottom topography $z = -h(x)$. The total number N of the spectral approximation in (5.7) and the time increment Δt of the fourth-order Runge–Kutta scheme for the evolution equations are set to $N = 2048$ and $\Delta t = 0.05$, respectively. The threshold N_{filter} for the de-aliasing filter in (5.8) is set to $N_{filter} = 900$ for SNL and $N_{filter} = 400$ for WNL and FNL.

Figures 2(*a*), 2(*b*) and 2(*c*) show the computed results of time evolution of the wave profile $z = \zeta(x, t)$ for $\tilde{\alpha}_0 = 0.05$, 0.07 and 0.09, respectively, where $\tilde{\alpha}_0 = H_0/h_0$ denotes the wave height of the initial cnoidal wave (5.12). Figures 2(*b* i) and 2(*b* ii) enlarge (*b*) at $t = 45$ and 54, respectively, and figures 2(*c* i) and 2(*c* ii) enlarge (*c*) at $t = 45$ and 54, respectively. Figures 3(*a*), 3(*b*), 3(*c*) and 3(*d*) compare the three-dimensional plots in the (x, t, z) space of time evolution of the wave profile $z = \zeta(x, t)$ for $\tilde{\alpha}_0 = 0.09$ using the first- and second-order SNL, WNL and FNL models, respectively. The wave height increases as the wave approaches the hump of the bottom, and the long cnoidal wave

https://doi.org/10.1017/jfm.2026.11135 Published online by Cambridge University Press

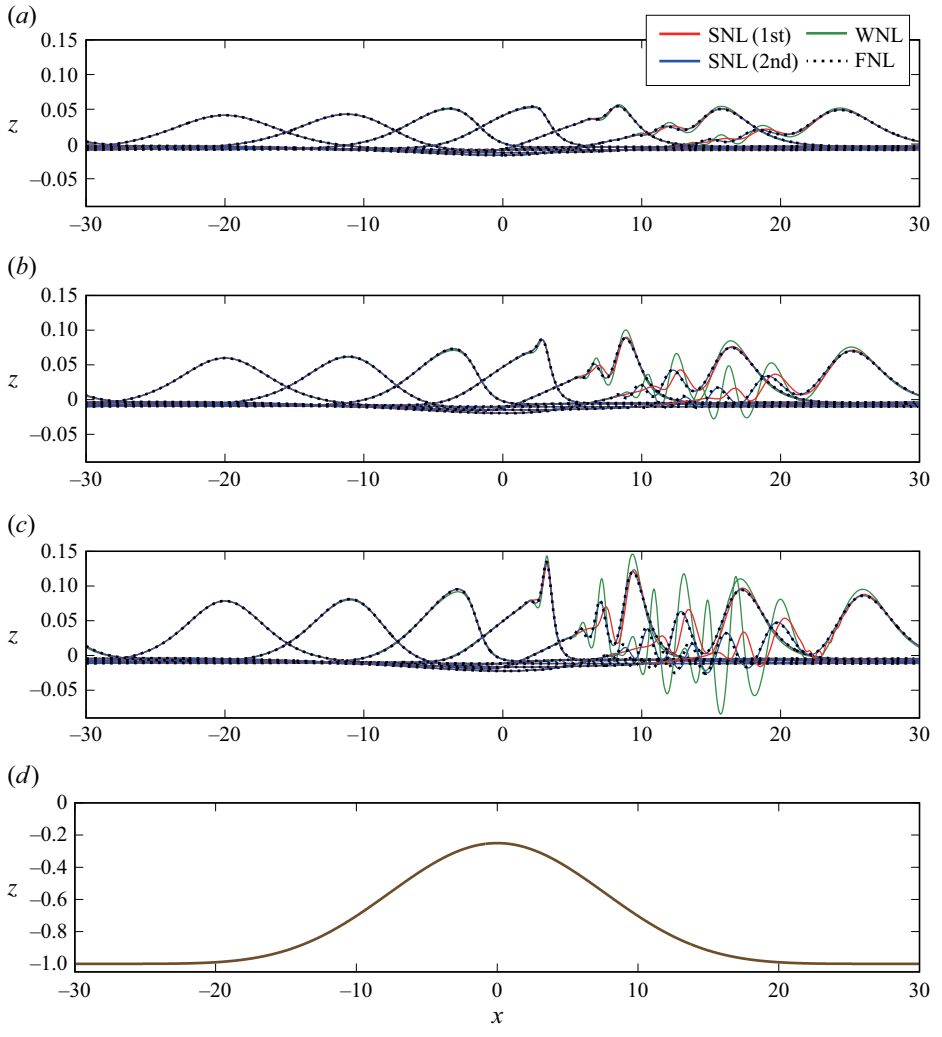


Figure 2. For caption see next page.

disintegrates into several shorter waves or rank-ordered solitary waves after travelling over the top of the hump at $x = 0$. Compared with the FNL computation, it is found that the second-order SNL model produces more accurate solutions in this range of the height $\tilde{\alpha}_0$ than the first-order SNL and WNL models, which fail to capture the disintegration process correctly. It should be noted that the shorter waves generated by the first-order SNL model propagate faster than those of the second-order SNL model or the FNL solutions. This seems to be related to the linear dispersion relation of the SNL models. The full linear dispersion relation for small-amplitude sinusoidal waves with the wavenumber k and the wave frequency ω propagating on water of constant depth h_0 is given by

$$\omega^2 = gk \tanh kh_0 \quad \text{or} \quad \frac{c^2}{gh_0} = \frac{\tanh kh_0}{kh_0} \quad \text{with} \quad c = \frac{\omega}{k}. \tag{5.18}$$

For long waves with $kh_0 \ll 1$, this dispersion relation is approximated by the Mth order SNL model as (Choi 2022*a*, (2.16))

https://doi.org/10.1017/jfm.2026.11135 Published online by Cambridge University Press

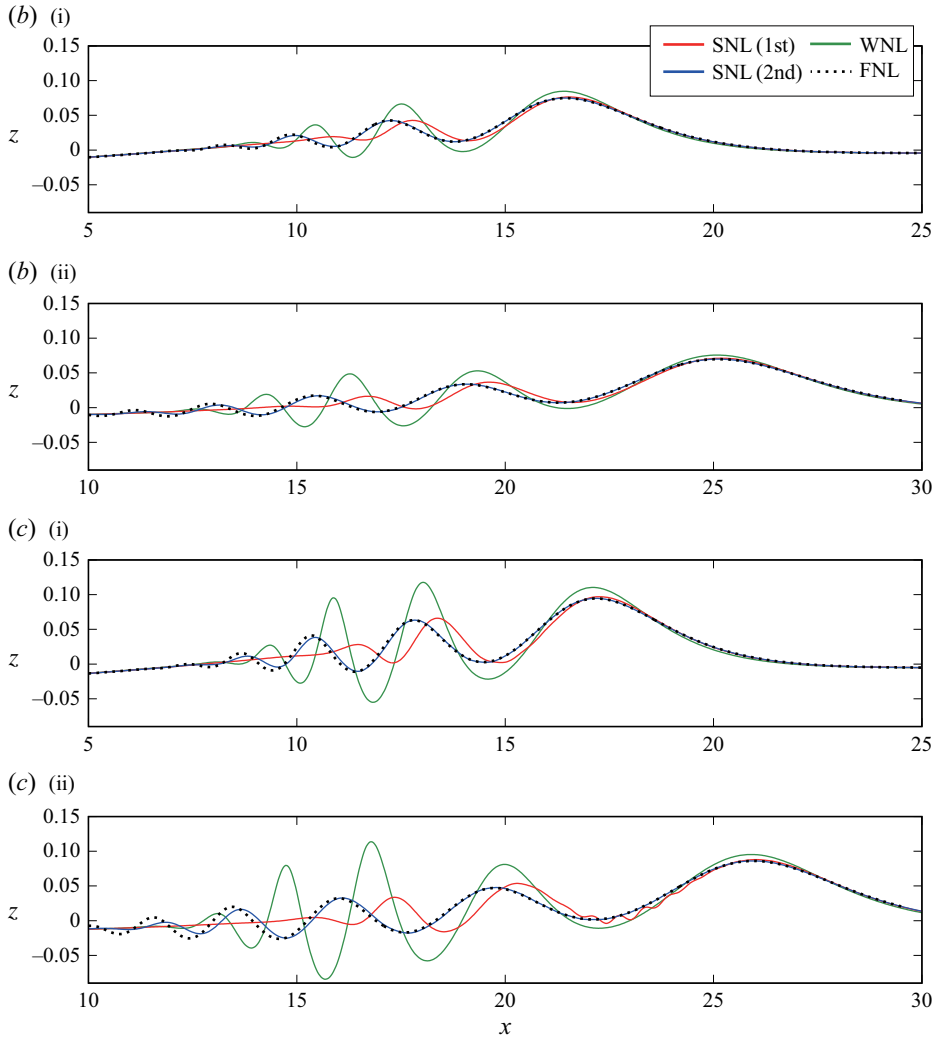


Figure 2. (cntd). Comparison of the time evolution of the wave profile $z=\zeta(x,t)$ of example 1. The wave profiles $z=\zeta(x,t)$ at $t=0$, 9, 18, 27, 36, 45 and 54 are plotted in each figure. The initial wave profile $\zeta(x,t=0)$ is given by (5.12) with $L=60$ and $x_0=-20$ for (*a*) $\tilde{\alpha}_0=0.05$, (*b*) $\tilde{\alpha}_0=0.07$ and (*c*) $\tilde{\alpha}_0=0.09$, where $\tilde{\alpha}_0=H_0/h_0$ denotes the dimensionless wave height of the initial wave. The red line —— represents the first-order SNL long wave model, the blue line —— the second-order SNL model, the green line —— the WNL long wave model and the black dashed line - - - - the FNL computation. The brown line —— in (*d*) shows the shape of the bottom topography $h(x)$ given by (5.16) with $h_b=0.75$ and $q_{\ell_b}=0.01$. The time increment Δt of the fourth-order Runge–Kutta scheme, the total number N of the spectral approximation in (5.7) and the threshold N_{filter} for the de-aliasing filter in (5.8) are set to $\Delta t=0.05$, $N=2048$ and $N_{filter}=900$ (SNL) and 400 (WNL and FNL), respectively. Panels (*b* i) and (*b* ii) enlarge (*b*) at $t=45$ and 54, respectively. Panels (*c* i) and (*c* ii) enlarge (*c*) at $t=45$ and 54, respectively.

$$\omega^2=gh_0k^2\cdot\frac{1+\sum_{m=1}^{M}\dfrac{(kh_0)^{2m}}{(2m+1)!}}{1+\sum_{m=1}^{M}\dfrac{(kh_0)^{2m}}{(2m)!}}\quad\text{or}\quad\frac{c^2}{gh_0}=\frac{1+\sum_{m=1}^{M}\dfrac{(kh_0)^{2m}}{(2m+1)!}}{1+\sum_{m=1}^{M}\dfrac{(kh_0)^{2m}}{(2m)!}}.\tag{5.19}$$

https://doi.org/10.1017/jfm.2026.11135 Published online by Cambridge University Press

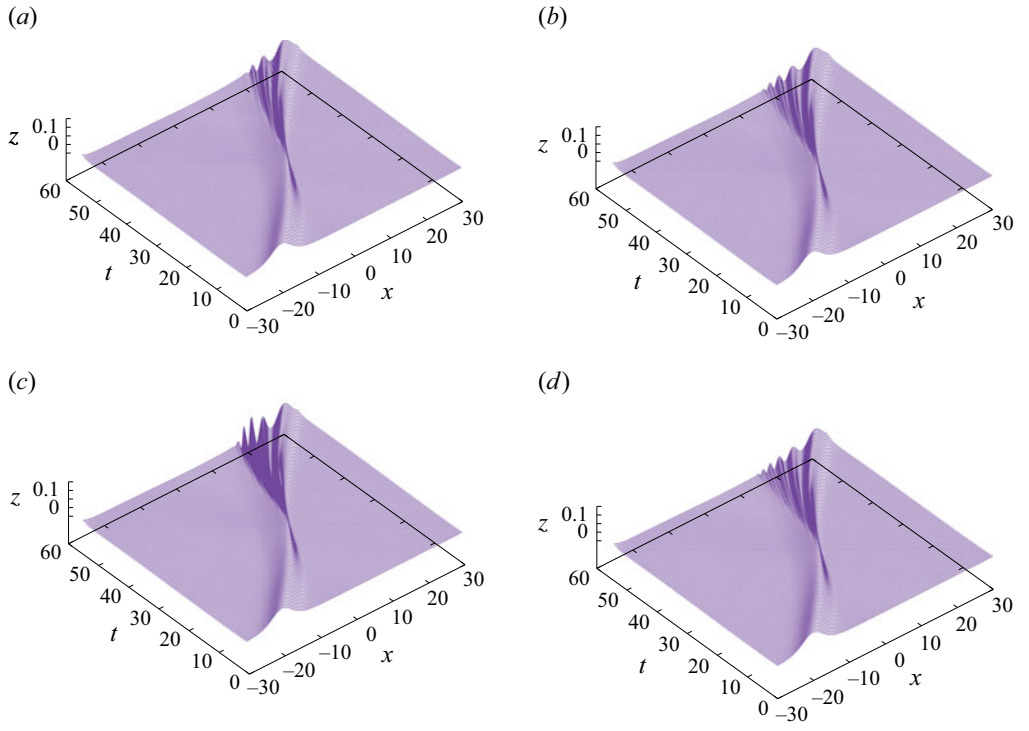


Figure 3. Three-dimensional plot for the time evolution of the wave profile $z = \zeta(x, t)$ of example 1 for $\tilde{\alpha}_0 = 0.09$ in the (x, t, z) space. The time interval is 0.5. For further information, see the caption of figure 2. (*a*) First-order SNL, (*b*) second-order SNL, (*c*) WNL, (*d*) FNL.

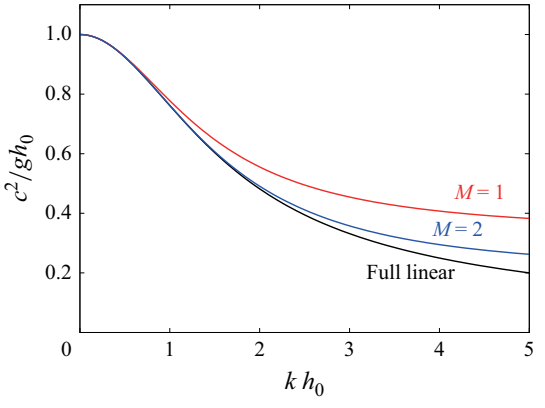


Figure 4. Variation of the wave speed squared c^2/gh_0 with the dispersion parameter kh_0 in the linear dispersion relations. The black line —— represents the full linear dispersion relation (5.18). The red line —— and blue line —— denote the linear dispersion relation (5.19) with $M = 1$ (first-order SNL) and $M = 2$ (second-order SNL), respectively.

Figure 4 compares the variation of $c^2/(gh_0)$ with the dispersion parameter kh_0 in (5.18) and (5.19) with $M = 1$ and 2. We can see that the linear wave speed for the second-order SNL model ($M = 2$) agrees with that of the Euler equations for $kh_0 < 2$, while the agreement for the first-order SNL model ($M = 1$) is observed for $kh_0 < 1$. The wave speed

https://doi.org/10.1017/jfm.2026.11135 Published online by Cambridge University Press

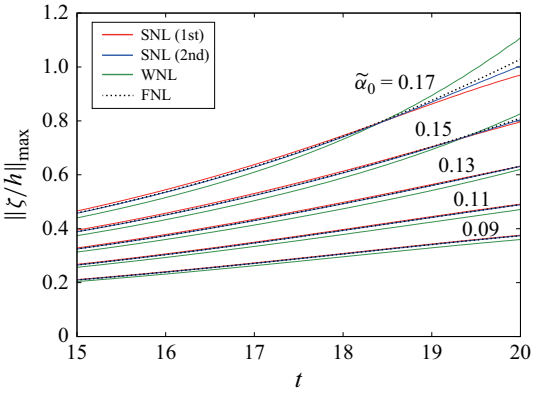


Figure 5. Variation of the shoaling rate $\|\zeta/h\|_{\max}$ on the up-slope with time t (example 1). Each numeral in the figure shows the value of the height $\tilde{\alpha}_0 = H_0/h_0$ of the initial wave (5.12). The shoaling rate $\|\zeta/h\|_{\max}$ is defined by (5.20). The red line —— represents the first-order SNL long wave model, the blue line —— the second-order SNL model, the green line —— the WNL long wave model and the black dashed line - - - - the FNL computation. For further information, see the caption of figure 2.

for the first-order model is always greater than that of the second-order or FNL model, as observed in our numerical results. Therefore, one can conclude that the short-wavelength behaviour is captured better by increasing the order of approximation.

Figure 5 shows the variation of the shoaling rate $\|\zeta/h\|_{\max}$ for $15 \leqslant t \leqslant 20$ when the crests of incident waves ($\tilde{\alpha}_0 = 0.09$, 0.11, 0.13, 0.15 and 0.17) are on the up-slope, where

$$\left\| \frac{\zeta}{h} \right\|_{\max} := \max_{-L/2 \leqslant x \leqslant L/2} \left| \frac{\zeta(x,t)}{h(x)} \right|. \tag{5.20}$$

The results show that, for the bottom topography given by (5.16), the second-order SNL model better approximates the shoaling rate $\|\zeta/h\|_{\max}$ of the FNL solution for $\|\zeta/h\|_{\max} < 0.8$ than the first-order SNL and WNL models.

5.3. *Example 2: forced generation of solitary waves by a bottom topography moving steadily with a transcritical speed*

As mentioned in § 1, a submerged hump moving steadily with a transcritical speed in a layer of shallow water, as shown in figure 1(*b*), can generate a succession of solitary waves propagating ahead of the hump. In this example, we perform numerical computation for this phenomenon, namely the forced generation of solitary waves by a bottom topography moving to the negative x direction with constant speed U in water of finite depth h_0, using the proposed SNL models. The bottom topography $z = -h(x,t)$ in the non-dimensional form is given by

$$h(x,t) = 1 - h_b \operatorname{sech}^2 k_b X \quad \text{with} \quad X = x + F_r t, \tag{5.21}$$

where the Froude number F_r is defined by

$$F_r = U/\sqrt{g h_0}. \tag{5.22}$$

Then it is convenient to consider this problem in the (X,t) frame of reference moving with the bottom topography, instead of the (x,t) frame, where $X = x + F_r t$. The Froude number F_r and k_b in (5.21) are fixed to $F_r = 1.01$ and $k_b = 0.5$, respectively. The X domain for computation is set to $-250 \leqslant X \leqslant 250$ ($L = 500$) and other parameters are $N = 2048$ and $\Delta t = 0.05$.

https://doi.org/10.1017/jfm.2026.11135 Published online by Cambridge University Press

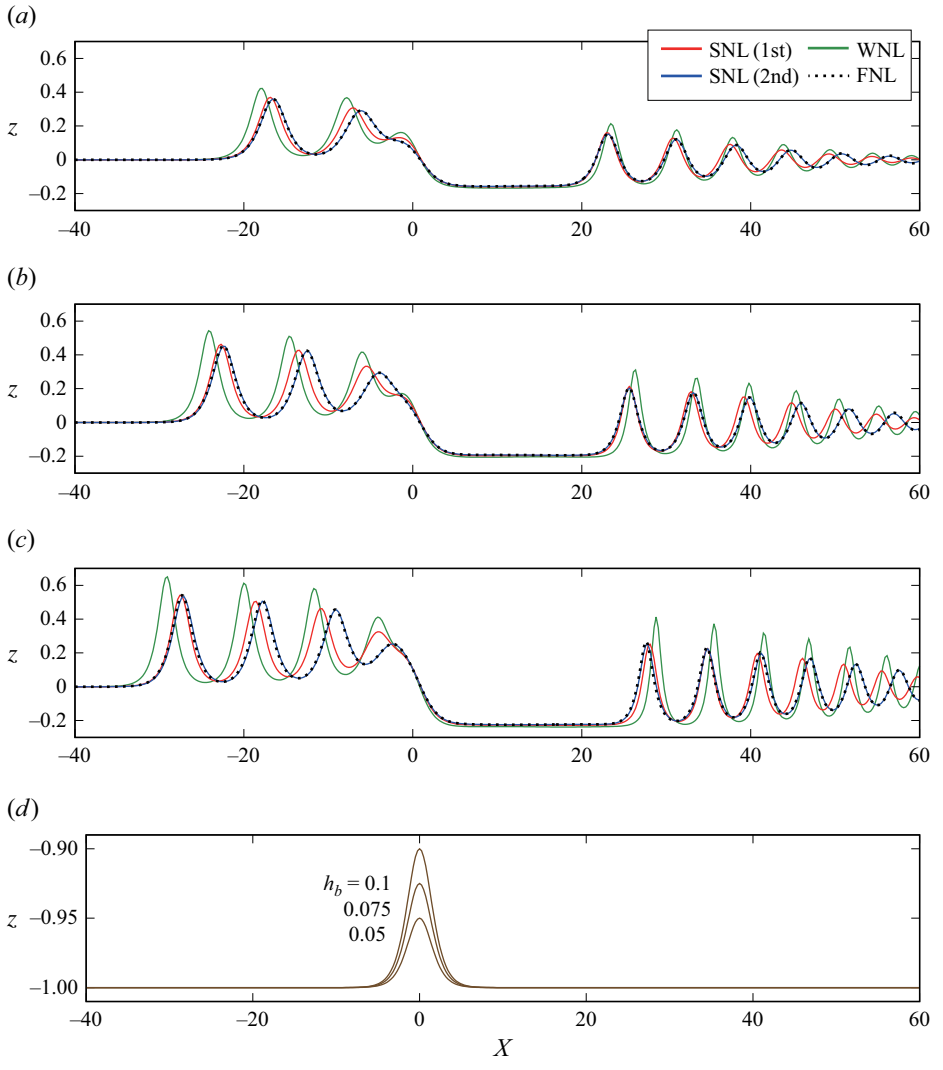


Figure 6. Comparison of the wave profile $z = \zeta(X, t)$ at $t = 150$ for example 2. Here $X = x + F_r t$. The height h_b of the bottom topography $z = -h(x, t) = -h(X)$ in (5.21) is set as (a) 0.05, (b) 0.075 and (c) 0.1. The Froude number F_r and k_b in (5.21) are fixed to $F_r = 1.01$ and $k_b = 0.5$, respectively. The red line —— represents the first-order SNL long wave model, the blue line —— the second-order SNL model, the green line —— the WNL long wave model and the black dashed line - - - - the FNL. The brown line —— in (d) shows the shape of the bottom topography moving to the left. Here $L = 500$, $\Delta t = 0.05$ and $N = 2048$ with $N_{filter} = 500$ (SNL), 320 (WNL) and 400 (FNL).

Figures 6(a), 6(b) and 6(c) show the computed results of the wave profiles $z = \zeta(X, t)$ at $t = 150$ for $h_b = 0.05$, 0.075 and 0.1, respectively, where h_b denotes the height of the bottom topography in (5.21). The shape of the bottom topography is shown in figure 6(d). Figures 7(a), 7(b), 7(c) and 7(d) compare the three-dimensional plots in the (X, t, z) space of time evolution of the wave profile $z = \zeta(X, t)$ for $h_b = 0.1$ using the first- and second-order SNL, WNL and FNL models, respectively. All three long wave models predicts the generation of solitary waves propagating ahead of the hump, but, when compared with the FNL computations, the second-order SNL model produces the most accurate results.

https://doi.org/10.1017/jfm.2026.11135 Published online by Cambridge University Press

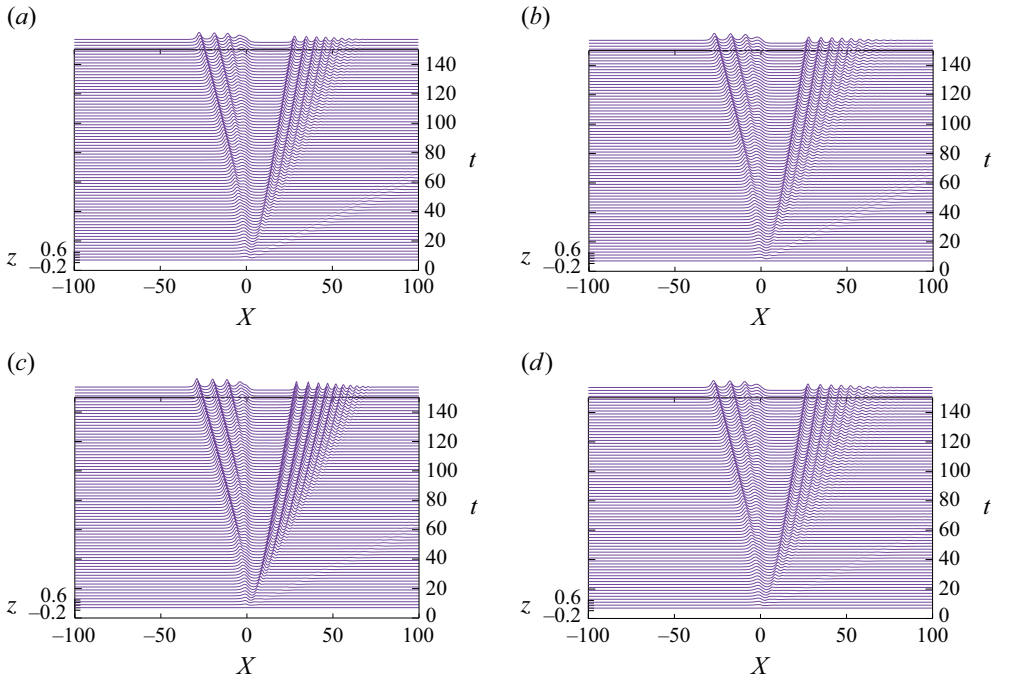


Figure 7. Three-dimensional plot of the time evolution of the wave profile $z = \zeta(X, t)$ for $F_r = 1.01$ and $h_b = 0.1$ in the (X, t, z) space of example 2. Here $X = x + F_r t$. The time interval is 2.0. For further information, see the caption of figure 6. (*a*) First-order SNL, (*b*) second-order SNL, (*c*) WNL, (*d*) FNL.

	SNL (1st)	SNL (2nd)	WNL	FNL
Example 1 ($\tilde{\alpha}_0 = 0.09$, $0 \leqslant t \leqslant 54$)	299	319	297	3273
Example 2 ($h_b = 0.1$, $0 \leqslant t \leqslant 150$)	816	878	837	9866

Table 1. Comparison of CPU time to solve each model. Numerical computations were performed using a MacBook Pro with an Apple M4 Pro. The unit of CPU time is seconds. Here SNL (1st) and SNL (2nd) denote the first- and second-order SNL long wave models, respectively. See captions of figures 2 and 6 for details of numerical computations.

Table 1 summarises the CPU time of each model for example 1 ($\tilde{\alpha}_0 = 0.09$) and example 2 ($h_b = 0.1$) for the computations using a MacBook Pro with an Apple M4 Pro. Note that the CPU time for each long wave model (SNL and WNL) is less than 1/10 of that for the FNL model and no significant increase of the CPU time is observed for the second-order model compared with the first-order model.

From these two numerical examples, one can conclude that the high-order terms in the SNL models should be included to better describe the evolution of nonlinear long waves in the presence of a variable bottom.

6. Conclusions

We have developed the SNL long wave model for a variable bottom with generalising the model proposed by Choi (2022*a*) for a flat bottom. Under the assumption that $\beta = h_0/\lambda_0 \ll 1$ and $|\nabla h| = O(\beta)$, by expanding the velocity potential ϕ and the vertical

https://doi.org/10.1017/jfm.2026.11135 Published online by Cambridge University Press

velocity w at the bottom $z=-h(\boldsymbol{x},t)$, we have presented a system of nonlinear evolution equations (4.1) for the surface elevation ζ and the bottom velocity $\boldsymbol{v}=\nabla\phi_b$ that is valid at any order of approximation in β^2.

In order to examine their performance with a variable bottom, the first- and second-order SNL models given by (5.2) and (5.3), respectively, are solved numerically using a pseudo-spectral method for the deformation and generation of long waves over a bottom topography. When compared with the FNL computations using the boundary integral method in Appendix D, the computed results in §§ 5.2 and 5.3 have shown that the second-order SNL model produces more accurate results than the first-order SNL model and the WNL model. This demonstrates the importance of high-order (both linear and nonlinear) dispersive effects that cannot be stably described by many of the widely used long wave models for the depth-averaged velocity or the velocity at a fixed vertical level due to the instability or the ill-posedness caused by truncation of the linear dispersion relation for water waves. Therefore, it can be concluded that the high-order SNL model for the bottom velocity removes these non-physical artefacts even in the presence of bottom topography.

Acknowledgements. The authors are grateful to the reviewers for their constructive feedback and insightful comments, which have significantly improved this work.

Funding. The work of W.C. was supported by the US National Science Foundation through grant number DMS-2108524. The work of S.M. was supported by JSPS KAKENHI Grant-in-Aid grant number JP23K22407.

Declaration of interests. The authors report no conflict of interest.

Appendix A. Explicit expressions for expanded variables

Here we present the explicit expressions for expanded variables that are necessary to write the evolution equations valid to $O(\beta^4)$. From (3.9*a*) and (3.9*b*), the expressions for $\phi_{2j,2m}$ $(j,m=0,1)$ are given by

$$\phi_{0,0}=\phi_b,\quad \phi_{0,2}=0,\quad \phi_{0,4}=0, \tag{A1a}$$

$$\phi_{2,0}=\nabla^2\phi_{0,0}=\nabla^2\phi_b,\quad \phi_{4,0}=\nabla^2\phi_{2,0}=\nabla^4\phi_b, \tag{A1b}$$

$$\begin{aligned}\phi_{2,2}&=\nabla^2\phi_{0,2}-|\nabla h|^2\nabla^2\phi_{0,0}+2\nabla w_{0,0}\cdot\nabla h+w_{0,0}\nabla^2 h\\&=-|\nabla h|^2\nabla^2\phi_b-2\nabla\dot{h}\cdot\nabla h-\dot{h}\nabla^2 h=-\Pi,\end{aligned} \tag{A1c}$$

while those for $w_{2j,2m}$ are given, from (3.9*c*), by

$$w_{0,0}=-\dot{h},\quad w_{0,2}=|\nabla h|^2\dot{h},\quad w_{0,4}=-|\nabla h|^4\dot{h}, \tag{A2a}$$

$$\begin{aligned}w_{2,0}&=\nabla^2 w_{0,0}-2\nabla\phi_{2,0}\cdot\nabla h-\phi_{2,0}|\nabla h|^2\\&=-\nabla^2\dot{h}-2\nabla^2(\nabla\phi_b)\cdot\nabla h-(\nabla^2\phi_b)(\nabla^2 h)=-\Omega.\end{aligned} \tag{A2b}$$

By substituting these into (3.11*a*) and (3.11*b*), the expressions for Φ_{2m} $(m=0,1,2)$ can be found as

$$\Phi_0=\phi_b, \tag{A3a}$$

$$\Phi_2=\phi_{0,2}-\frac{\eta^2}{2!}\phi_{2,0}+\eta w_{0,0}=-\frac{\eta^2}{2!}\nabla\phi_b-\eta\dot{h}, \tag{A3b}$$

$$\begin{aligned}\Phi_4&=\phi_{0,4}-\frac{\eta^2}{2!}\phi_{2,2}+\frac{\eta^4}{4!}\phi_{4,0}+\eta w_{0,2}-\frac{\eta^3}{3!}w_{2,0}\\&=\frac{\eta^4}{4!}\nabla^4\phi_b+\frac{\eta^3}{3!}\Omega+\frac{\eta^2}{2!}\Pi+\eta|\nabla h|^2\dot{h}.\end{aligned} \tag{A3c}$$

https://doi.org/10.1017/jfm.2026.11135 Published online by Cambridge University Press

On the other hand, from (3.11*c*), W_{2m} ($m = 0, 1$) are given by

$$W_0 = -\eta\phi_{2,0} + w_{0,0} = -\eta\nabla^2\phi_b - \dot{h}, \tag{A4a}$$

$$W_2 = -\eta\phi_{2,2} + w_{0,2} + \frac{\eta^3}{3!}\phi_{4,0} - \frac{\eta^2}{2!}w_{2,0} = \frac{\eta^3}{3!}\nabla^4\phi_b + \frac{\eta^2}{2!}\Omega + \eta\Pi + |\nabla h|^2\dot{h}. \tag{A4b}$$

Then, the right-hand sides of the evolution equations, or Q_{2m} and R_{2m}, can be obtained from (4.2) and (4.3) although Q_{2m} can be found more conveniently, from (4.5), as

$$Q_0 = -\boldsymbol{\nabla}\cdot(\eta\overline{\boldsymbol{u}}_0) - h_t, \quad Q_{2m} = -\boldsymbol{\nabla}\cdot(\eta\overline{\boldsymbol{u}}_{2m}), \tag{A5a,b}$$

where $\overline{u}_{2m}$ are expressed, in terms of ζ and v, in (B4). On the other hand, R_{2m} ($m = 0, 1, 2$) can be obtained, from (4.3) with (A3) and (A4), as

$$R_0 = -g\zeta - \frac{1}{2}|\nabla\Phi_0|^2 = -g\zeta - \frac{1}{2}|\nabla\phi_b|^2, \tag{A6a}$$

$$R_2 = -\nabla\Phi_0\cdot\nabla\Phi_2 + \frac{1}{2}{W_0}^2 = \boldsymbol{\nabla}\cdot\left(\frac{\eta^2}{2!}\nabla^2\phi_b\nabla\phi_b\right) + \boldsymbol{\nabla}\cdot(\eta\dot{h}\nabla\phi_b) + \frac{1}{2}\dot{h}^2, \tag{A6b}$$

$$R_4 = -\frac{1}{2}(2\nabla\Phi_0\cdot\nabla\Phi_4 + \nabla\Phi_2\cdot\nabla\Phi_2) + W_0W_2 + \frac{1}{2}|\nabla\zeta|^2{W_0}^2 = -\left[\boldsymbol{v}\cdot\nabla\Phi_4 + \frac{1}{2}\left|\nabla\left(\frac{\eta^2}{2!}\boldsymbol{\nabla}\cdot\boldsymbol{v} + \eta\dot{h}\right)\right|^2 + W_2(\eta\boldsymbol{\nabla}\cdot\boldsymbol{v} + \dot{h}) - \frac{1}{2}|\nabla\zeta|^2(\eta\boldsymbol{\nabla}\cdot\boldsymbol{v} + \dot{h})^2\right], \tag{A6c}$$

where W_2 and Φ_4 are defined in (4.22) with Ω and Π given by (4.23).

Appendix B. Expansion for the depth-averaged velocity

From (4.4), the depth-averaged velocity $\overline{\boldsymbol{u}}$ is given by

$$\eta\overline{\boldsymbol{u}} = \boldsymbol{\nabla}\left(\int_{-h}^{\zeta}\phi\,\mathrm{d}z\right) - \Phi\nabla\zeta - \phi_b\nabla h = \boldsymbol{\nabla}\left[\sum_{j=0}^{\infty}\left\{\frac{(-1)^j\eta^{2j}}{(2j)!}\phi_{2j} + \frac{(-1)^j\eta^{2j+1}}{(2j+1)!}w_{2j}\right\}\right] - \Phi\nabla\zeta - \phi_b\nabla h. \tag{B1}$$

As ϕ_{2j}, w_{2j} and Φ can be expanded in β^2, as shown in (3.6*a*), (3.6*b*) and (3.10*a*), respectively, $\overline{\boldsymbol{u}}$ can also be expanded as

$$\overline{\boldsymbol{u}} = \sum_{m=0}^{\infty}\overline{\boldsymbol{u}}_{2m}, \tag{B2}$$

where $\overline{\boldsymbol{u}}_{2m} = O(\beta^{2m})$ can be found from

$$\eta\overline{\boldsymbol{u}}_0 = \boldsymbol{\nabla}(\eta\phi_b) - \phi_b\boldsymbol{\nabla}\eta = \eta\boldsymbol{\nabla}\phi_b = \eta\boldsymbol{v}, \tag{B3a}$$

$$\eta\overline{\boldsymbol{u}}_{2m} = \boldsymbol{\nabla}\left[\sum_{n=0}^{m-1}\left\{\frac{(-1)^{n+1}}{(2n+3)!}\eta^{2n+3}\phi_{2n+2,2(m-n-1)} + \frac{(-1)^n}{(2n+2)!}\eta^{2n+2}w_{2n,2(m-n-1)}\right\}\right] - \Phi_{2m}\boldsymbol{\nabla}\zeta. \tag{B3b}$$

https://doi.org/10.1017/jfm.2026.11135 Published online by Cambridge University Press

By substituting (3.11*b*) for Φ_{2m} into (B3*b*), one can find that $\overline{\boldsymbol{u}}_0 = \boldsymbol{v}$ while $\overline{\boldsymbol{u}}_{2m}$ ($m \geqslant 1$) are given by

$$\overline{\boldsymbol{u}}_{2m} = \sum_{n=0}^{m-1} \left[\frac{(-1)^{n+1}}{(2n+3)!} \eta^{2n+2} \phi_{2n+2,2(m-n-1)} + \frac{(-1)^n}{(2n+2)!} \eta^{2n+1} w_{2n,2(m-n-1)} \right] + \sum_{n=0}^{m-1} \left[\frac{(-1)^{n+1}}{(2n+2)!} \eta^{2n+1} \phi_{2n+2,2(m-n-1)} + \frac{(-1)^n}{(2n+1)!} \eta^{2n} w_{2n,2(m-n-1)} \right] \boldsymbol{\nabla} h, \tag{B4}$$

where $\phi_{2n,2m}$ and $w_{2n,2m}$ are defined by (3.9). For example, the expressions for $\overline{\boldsymbol{u}}_{2m}$ for $m = 0, 1, 2$ are given explicitly by

$$\overline{\boldsymbol{u}}_0 = \boldsymbol{v}, \tag{B5a}$$

$$\begin{aligned} \overline{\boldsymbol{u}}_2 &= -\frac{\eta^2}{3!} \boldsymbol{\nabla} \phi_{2,0} + \frac{\eta}{2!} \boldsymbol{\nabla} w_{0,0} + \left(-\frac{\eta}{2} \phi_{2,0} + w_{0,0} \right) \boldsymbol{\nabla} h \\ &= -\frac{\eta^2}{3!} \nabla^2 \boldsymbol{v} - \frac{\eta}{2!} \boldsymbol{\nabla} \dot{h} - \left(\frac{\eta}{2} \boldsymbol{\nabla} \boldsymbol{\cdot} \boldsymbol{v} + \dot{h} \right) \boldsymbol{\nabla} h, \end{aligned} \tag{B5b}$$

$$\begin{aligned} \overline{\boldsymbol{u}}_4 &= \frac{\eta^4}{5!} \boldsymbol{\nabla} \phi_{4,0} - \frac{\eta^2}{3!} \boldsymbol{\nabla} \phi_{2,2} - \frac{\eta^3}{4!} \boldsymbol{\nabla} w_{2,0} + \frac{\eta}{2!} \boldsymbol{\nabla} w_{0,2} \\ &\quad + \left(\frac{\eta^3}{4!} \phi_{4,0} - \frac{\eta}{2!} \phi_{4,0} - \frac{\eta^2}{3!} w_{2,0} + w_{0,2} \right) \boldsymbol{\nabla} h \\ &= \frac{\eta^4}{5!} \nabla^4 \boldsymbol{v} + \frac{\eta^3}{4!} \boldsymbol{\nabla} \Omega + \frac{\eta^2}{3!} \boldsymbol{\nabla} \Pi + \frac{\eta}{2!} \boldsymbol{\nabla} (|\boldsymbol{\nabla} h|^2 \dot{h}) + \frac{1}{\eta} \Phi_4 \boldsymbol{\nabla} h, \end{aligned} \tag{B5c}$$

where Φ_4 are defined in (4.22*b*) with Ω and Π given by (4.23).

For the flat bottom, the expressions for $\overline{\boldsymbol{u}}_{2m}$ ($m \geqslant 0$) can be simplified (Choi 2022*a*) to

$$\overline{\boldsymbol{u}}_{2m} = \frac{(-1)^m}{(2m+1)!} \eta^{2m} \nabla^{2m} \boldsymbol{v}. \tag{B6}$$

Appendix C. The initial guess $v^{(0)}$ for the iterative scheme (5.10)

It may be natural to set the initial value $v^{(0)}(x, t)$ by linear extrapolation using the two previous times $t - \Delta t$ and $t - 2\Delta t$ as

$$v^{(0)}(x, t) = 2v(x, t - \Delta t) - v(x, t - 2\Delta t). \tag{C1}$$

However, the convergence of the iterative scheme (5.10) using the initial guess $v^{(0)}$ in (C1) is very slow, as shown in method 1 of figure 8.

On the other hand, we may approximate (5.9) by a system of simultaneous linear equations using the finite difference discretisation of the spatial differentiation of $v(x, t)$ with the error of $O(\Delta x^4)$ as

https://doi.org/10.1017/jfm.2026.11135 Published online by Cambridge University Press

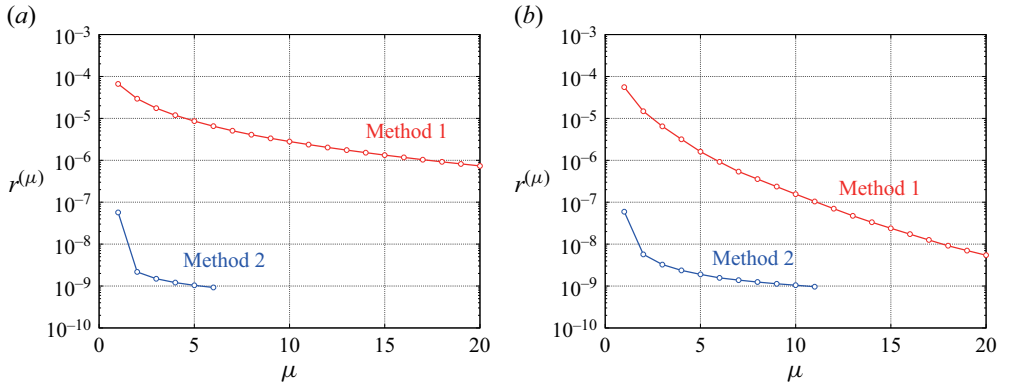


Figure 8. Convergence of the iterative scheme (5.10) for two different initial guesses $v^{(0)}$: the residual $r^{(\mu)}(t)$ versus the iteration number μ. Method 1 (red line ——): $v^{(0)}$ is given by the linear extrapolation (C1). Method 2 (blue line ——): $v^{(0)}$ is given by the finite difference approximation of (5.9). The residual $r^{(\mu)}(t)$ is defined by (5.11). The computed results are obtained using the second-order SNL model for example 1 with $\tilde{\alpha}_0 = 0.09$ in § 5.2. See the caption of figure 2 for other parameter values. Results are shown for (*a*) $t = 20$ and (*b*) $t = 50$.

$$\left.\begin{aligned} v_x(x_j,t) &\simeq \frac{v_{j-2} - 8v_{j-1} + 8v_{j+1} - v_{j+2}}{12\Delta x} \\ v_{xx}(x_j,t) &\simeq \frac{-v_{j-2} + 16v_{j-1} - 30v_j + 16v_{j+1} - v_{j+2}}{12\Delta x^2} \\ v_{xxx}(x_j,t) &\simeq \frac{v_{j-3} - 8v_{j-2} + 13v_{j-1} - 13v_{j+1} + 8v_{j+2} - v_{j+3}}{8\Delta x^3} \\ v_{xxxx}(x_j,t) &\simeq \frac{-v_{j-3} + 12v_{j-2} - 39v_{j-1} + 56v_j - 39v_{j+1} + 12v_{j+2} - v_{j+3}}{6\Delta x^4} \end{aligned}\right\}, \tag{C2}$$

with $v_j = v(x_j,t)$. Then we adopt a numerical solution of the simultaneous linear equations with the initial guess $v^{(0)}$ for the iterative scheme (5.10). Figure 8 shows that method 2 using this initial guess $v^{(0)}$ improves convergence of (5.10) considerably.

Appendix D. Fully nonlinear computation using a boundary integral method

This appendix summarises the method of FNL computation for free surface flow over a variable bottom, which is based on a boundary integral method developed by Baker *et al.* (1982). Here we assume that the bottom topography is time independent as $h = h(x)$ in (5.16) for example 1 and $h = h(x,t) = h(X)$ with $X = x + F_r t$ in (5.21) for example 2.

First, for the computational domain bounded by $-L/2 < x < L/2$ and $-h(x) < z < \zeta(x,t)$, we introduce the new complex spatial variables $Z = x + \mathrm{i}z$ and $\hat{\zeta} = \hat{\xi} + \mathrm{i}\hat{\eta}$ defined by

$$\hat{\zeta} = \frac{2\pi}{L} Z \quad \text{with } \hat{\xi} = \frac{2\pi}{L} x, \quad \hat{\eta} = \frac{2\pi}{L} z. \tag{D1}$$

Then the computational domain is given by

$$-\pi < \hat{\xi} < \pi \quad \text{and} \quad -\check{\eta}(x) < \hat{\eta} < \tilde{\eta}(x,t)\,, \tag{D2}$$

where $\check{\eta}(x) = (2\pi/L)h(x)$ and $\tilde{\eta}(x,t) = (2\pi/L)\zeta(x,t)$. From periodicity, we may parameterise each variable at the free surface $z = \zeta(x,t)$ and the bottom $z = -h(x)$ and

https://doi.org/10.1017/jfm.2026.11135 Published online by Cambridge University Press

write them, respectively, as

$$\hat{\zeta}_F(p,t) = \hat{\zeta} \quad \text{at } z = \zeta(x,t) \quad (-\pi \leqslant p \leqslant \pi), \tag{D3a}$$

$$\hat{\zeta}_B(p) = \hat{\zeta} \quad \text{at } z = -h(x) \quad (-\pi \leqslant p \leqslant \pi), \tag{D3b}$$

where $\hat{\zeta}_B(p) = \hat{\xi}_B(p) + \mathrm{i}\hat{\eta}_B(p) = p - \mathrm{i}\check{\eta}_B(p)$, namely

$$\hat{\xi}_B(p) = p, \quad \hat{\eta}_B(p) = -\check{\eta}_B(p) = -\check{\eta}(x = x_B(p)) \quad \text{with } x_B(p) = \frac{L}{2\pi}\hat{\xi}_B(p). \tag{D4}$$

Hereafter, the time dependence of each variable is omitted, such as $\hat{\zeta}_F(p)$ instead of $\hat{\zeta}_F(p,t)$, just for notational brevity if its explicit expression is not necessary. From Cauchy's integral formula and periodicity, we can write the complex velocity $w = w(\hat{\zeta})$ using the vortex-sheet strengths $\gamma_F(p)$ at the free surface and $\gamma_B(p)$ at the bottom, similarly to Baker *et al.* (1982, (4.2)), as

$$w(\hat{\zeta}) = \frac{1}{4\pi\mathrm{i}}\frac{2\pi}{L}\left\{\int_{-\pi}^{\pi}\gamma_F(p')\cot\left[\frac{1}{2}\{\hat{\zeta} - \hat{\zeta}_F(p')\}\right]\mathrm{d}p' + \mathrm{i}\int_{-\pi}^{\pi}\gamma_B(p')\cot\left[\frac{1}{2}\{\hat{\zeta} - \hat{\zeta}_B(p')\}\right]\mathrm{d}p'\right\}. \tag{D5}$$

Here note that $\gamma_F(p)$ and $\gamma_B(p)$ are both real and

$$w = \frac{\partial f}{\partial Z} = \frac{\partial f/\partial p}{\partial Z/\partial p} = \frac{2\pi}{L}\frac{\partial f/\partial p}{\partial \hat{\zeta}/\partial p}, \tag{D6}$$

where $f = \phi + \mathrm{i}\psi$ denotes the complex velocity potential. Equation (D5) yields the complex velocities $w_F(p)$ at the free surface and $w_B(p)$ at the bottom, respectively, as

$$w_F(p) = w(\hat{\zeta}_F(p)) = \frac{2\pi}{L}\left\{I_{F1}(p) + I_{B1}(p) + \frac{1}{2}\frac{\gamma_F(p)}{\partial\hat{\zeta}_F/\partial p(p)}\right\}, \tag{D7a}$$

$$w_B(p) = w(\hat{\zeta}_B(p)) = \frac{2\pi}{L}\left\{I_{F2}(p) + I_{B2}(p) - \mathrm{i}\frac{1}{2}\frac{\gamma_B(p)}{\partial\hat{\zeta}_B/\partial p(p)}\right\}, \tag{D7b}$$

with

$$I_{F1}(p) = \frac{1}{4\pi\mathrm{i}}\mathrm{P.V.}\int_{-\pi}^{\pi}\gamma_F(p')\cot\left[\frac{1}{2}\{\hat{\zeta}_F(p) - \hat{\zeta}_F(p')\}\right]\mathrm{d}p', \tag{D8a}$$

$$I_{B1}(p) = \frac{1}{4\pi}\int_{-\pi}^{\pi}\gamma_B(p')\cot\left[\frac{1}{2}\{\hat{\zeta}_F(p) - \hat{\zeta}_B(p')\}\right]\mathrm{d}p', \tag{D8b}$$

$$I_{F2}(p) = \frac{1}{4\pi\mathrm{i}}\int_{-\pi}^{\pi}\gamma_F(p')\cot\left[\frac{1}{2}\{\hat{\zeta}_B(p) - \hat{\zeta}_F(p')\}\right]\mathrm{d}p', \tag{D8c}$$

$$I_{B2}(p) = \frac{1}{4\pi}\mathrm{P.V.}\int_{-\pi}^{\pi}\gamma_B(p')\cot\left[\frac{1}{2}\{\hat{\zeta}_B(p) - \hat{\zeta}_B(p')\}\right]\mathrm{d}p', \tag{D8d}$$

where P.V. denotes Cauchy's principal value.

The kinematic condition at the free surface is given by

$$\frac{\partial Z_F}{\partial t} = \overline{w}_F \quad \text{or} \quad \frac{\partial\hat{\zeta}_F}{\partial t} = \frac{2\pi}{L}\overline{w}_F, \tag{D9}$$

where $Z_F = Z_F(p,t) = x_F(p,t) + \mathrm{i}\,z_F(p,t)$, $\hat{\zeta}_F = \hat{\zeta}_F(p,t) = \hat{\xi}_F(p,t) + \mathrm{i}\,\hat{\eta}_F(p,t)$ and $\overline{w}$ denotes the complex conjugate of w. Taking the derivative of the dynamic condition at

https://doi.org/10.1017/jfm.2026.11135 Published online by Cambridge University Press

the free surface given by Bernoulli's equation with respect to p along the free surface, we obtain

$$\frac{\partial}{\partial t}\left(\frac{\partial \phi_F}{\partial p}\right) - \frac{1}{2}\frac{\partial}{\partial p}(w_F \overline{w}_F) + \frac{L}{2\pi}\frac{\partial \hat{\eta}_F}{\partial p} = 0\,, \tag{D10}$$

where ϕ_F denotes the velocity potential at the free surface and

$$\frac{\partial \phi_F}{\partial p} = \mathrm{Re}\left\{\frac{\partial f_F}{\partial p}\right\} = \mathrm{Re}\left\{\frac{\partial Z_F}{\partial p}\cdot w_F\right\}. \tag{D11}$$

The bottom condition is given by

$$\frac{\partial \psi_B}{\partial p} = 0, \tag{D12}$$

where ψ_B denotes the streamfunction at the bottom and

$$\frac{\partial \psi_B}{\partial p} = \mathrm{Im}\left\{\frac{\partial f_B}{\partial p}\right\} = \mathrm{Im}\left\{\frac{\partial Z_B}{\partial p}\cdot w_B\right\}. \tag{D13}$$

Note that (D7*a*) and (D11) yield

$$\gamma_F(p) \quad = 2\left[\frac{\partial \phi_F}{\partial p} - \mathrm{Re}\left\{\frac{\partial \hat{\zeta}_F}{\partial p}\cdot\{I_{F1}(p) + I_{B1}(p)\}\right\}\right]. \tag{D14}$$

Similarly, (D7*b*) and (D13) with (D12) produce

$$\gamma_B(p) \quad = 2\cdot \mathrm{Im}\left\{\frac{\partial \hat{\zeta}_B}{\partial p}\cdot\{I_{F2}(p) + I_{B2}(p)\}\right\}. \tag{D15}$$

In this work, we choose $\hat{\zeta}_F$ and $\partial\phi_F/\partial p$ as the dependent variables, and apply a pseudo-spectral method to the numerical computation of (D9) and (D10), similarly to that for the long wave models in § 5.1. For this, we need to obtain w_F included in (D9) and (D10), which is determined by γ_F and γ_B, as shown in (D7*a*). After solving the evolution equations (D9) for $\hat{\zeta}_F$ and (D10) for $\partial\phi_F/\partial p$, we can find γ_F and γ_B at a new time step as follows. The integrals in (D8) can be approximated using the trapezoidal rule and, in particular, Cauchy's principal value integrals in $I_{F1}(p)$ and $I_{B2}(p)$ can be approximated using the alternating trapezoidal rule (Beale, Hou & Lowengrub 1996, (6)). Then (D14) and (D15) are approximated by a system of simultaneous linear equations for γ_F and γ_B, which we numerically solve using the successive over-relaxation method.

To estimate the accuracy of this method of FNL computation, we monitor the wave energy $E(t)$, which is the sum of kinetic and potential energies, for the initial cnoidal wave (5.12) with a flat bottom $h = h_0$ ($L = 60$, $x_0 = -20$, $\Delta t = 0.05$, $N = 2048$ and $N_{filter} = 400$). Then it is found that, for the dimensionless wave height $\tilde{\alpha}_0 \leqslant 0.18$, the cnoidal waves propagates in almost permanent form with constant speed $\tilde{c}_0$ in (5.15) and the relative error $|E(t) - E(0)|/E(0) < 0.04\,\%$.

References

Baker, G.R., Meiron, D.I. & Orszag, S.A. 1982 Generalized vortex methods for free-surface flow problems. *J. Fluid Mech.* **123**, 477–501.

Beale, J., Hou, T.Y. & Lowengrub, J. 1996 Convergence of a boundary integral method for water waves. *SIAM J. Numer. Anal.* **33**, 1797–1843.

Chazel, F., Lannes, D. & Marche, F. 2010 Numerical simulation of strongly nonlinear and dispersive waves using a Green–Naghdi model. *J. Sci. Comput.* **48**, 105–116.

Choi, W. 2022*a* High-order strongly nonlinear long wave approximation and solitary wave solution. *J. Fluid Mech.* **945**, A15.

https://doi.org/10.1017/jfm.2026.11135 Published online by Cambridge University Press

CHOI, W. 2022*b* High-order strongly nonlinear long wave approximation and solitary wave solution. Part 2. Internal waves. *J. Fluid Mech.* **952**, A41.

CHOI, W. 2022*c* High-order strongly nonlinear long wave approximation and solitary wave solution - corrigendum. *J. Fluid Mech.* **952**, E2.

CRAIG, W. & SULEM, C. 1993 Numerical simulation of gravity waves. *J. Comput. Phys.* **108**, 73–83.

DINGEMANS, M.W. 1994 Comparison of computations with Boussinesq-like models and laboratory measurements. *Rep*. H-1684.12, 32. Delft Hydraulics.

DOMMERMUTH, D.G. & YUE, D.K.P. 1987 A high-order spectral method for the study of nonlinear gravity waves. *J. Fluid Mech.* **184**, 267–288.

GRILLI, S., SKOURUO, J. & SVENDSEN, I.A. 1989 An efficient boundary element method for nonlinear water waves. *Engng Anal. Bound. Elem.* **6**, 97–107.

GRIMSHAW, R., MALEEWONG, M. & ASAVANANT, J. 2009 Stability of gravity-capillary waves generated by a moving pressure disturbance in water of in finite depth. *Phys. Fluids* **21**, 082101.

GREEN, A.E. & NAGHDI, P.M. 1976 Derivation of equations for wave propagation in water of variable depth. *J. Fluid Mech.* **78**, 237–246.

JOHNSON, R.S. 1972 Some numerical solutions of a variable-coefficient Korteweg-de Vries equation (with applications to solitary wave development on a shelf). *J. Fluid Mech.* **54**, 81–91.

KAKUTANI, T. 1971 Effect of an uneven bottom on gravity waves. *J. Phys. Soc. Japan* **30**, 272–276.

LANNES, D. & MARCHE, F. 2015 A new class of fully nonlinear and weakly dispersive Green–Naghdi models for efficient 2D simulations. *J. Comput. Phys.* **282**, 238–268.

LEE, S.-J., YATES, G.T. & WU, T.Y. 1989 Experiments and analyses of upstream-advancing solitary waves generated by moving disturbances. *J. Fluid Mech.* **199**, 569–593.

MADSEN, P.A., BINGHAM, H.B. & LIU, H. 2002 A new Boussinesq method for fully nonlinear waves from shallow to deep water. *J. Fluid Mech.* **462**, 1–30.

MADSEN, P.A., FUHRMAN, D.R. & WANG, B. 2006 A Boussinesq-type method for fully nonlinear waves interacting with a rapidly varying bathymetry. *Coast. Engng* **53**, 487–504.

MADSEN, O.S. & MEI, C.C. 1969 The transformation of a solitary wave over an uneven bottom. *J. Fluid Mech.* **39**, 781–791.

MADSEN, O.S. & FUHRMAN, D.R. 2020 Trough instabilities in Boussinesq formulations for water waves. *J. Fluid Mech.* **889**, A38.

MATSUNO, Y. 2016 Hamiltonian structure for two-dimensional extended Green–Naghdi equations. *Proc. R. Soc. A* **472**, 20160127.

MEI, C.C. & LE MÉHAUTE, B. 1966 Note on the equations of long waves over an uneven bottom. *J. Geophys. Res.* **71**, 393–400.

PEREGRINE, D.H. 1967 Long waves on a beach. *J. Fluid Mech.* **27**, 815–827.

WEI, G., KIRBY, J.T., GRILLI, S.T. & SUBRAMANYA, R. 1995 A fully nonlinear Boussinesq model for surface waves. Part I. Highly nonlinear unsteady wave. *J. Fluid Mech.* **294**, 71–92.

WEST, B.J., BRUECKNER, K.A., JANDA, R.S., MILDER, D.M. & MILTON, R.L. 1987 A new numerical method for surface hydrodynamics. *J. Geophys. Res.* **92**, 11803–11824.

WU, T.Y. 1987 Generation of upstream advancing solitons by moving disturbances. *J. Fluid Mech.* **184**, 75–99.

WU, T.Y. & WU, D.M. 1982 Three-dimensional nonlinear long waves due to moving surface pressure. In *Proceeding of the 14th Symposium on Naval Hydrodynamics*, pp. 103–125. National Academy Press.

ZAKHAROV, V.E. 1968 Stability of periodic waves of finite amplitude on the surface of deep fluid. *J. Appl. Mech. Tech. Phys.* **9**, 190–194.

https://doi.org/10.1017/jfm.2026.11135 Published online by Cambridge University Press